Meng, Y. and B.G. Thomas, Metall. & Materials Trans. B, Vol. 34B, No. 5, Oct. 2003, pp. 707-725.

MODELING TRANSIENT SLAG LAYER PHENOMENA IN THE SHELL/MOLD GAP IN CONTINUOUS CASTING OF STEEL

Ya Meng and Brian G. Thomas

University of Illinois at Urbana-Champaign,
Department of Mechanical and Industrial Engineering,
1206 West Green Street, Urbana, IL USA 61801
Ph: 217-333-6919; Fax: 217-244-6534;
Email: yameng@uiuc.edu, bgthomas@uiuc.edu

ABSTRACT

Mold slag friction and fracture may cause heat transfer variations in continuous casting, which leads to steel shell temperature and stress variations, resulting in surface cracks. Analytical transient models of liquid slag flow and solid slag stress have been coupled with a finite-difference model of heat transfer in the mold, gap and steel shell to predict transient shear stress, friction, slip and fracture of the slag layers. The models are validated by comparing with numerical models and plant measurements of mold friction. Using reported slag fracture strength and TTT diagrams, the models are applied to study the effect of casting speed and mold powder viscosity properties on slag layer behavior between the oscillating mold wall and the solidifying steel shell. The study finds that liquid slag lubrication would produce negligible stresses. Lower mold slag consumption rate leads to high solid friction and results in solid slag layer fracture and movement below a critical value. Crystalline slag tends to fracture near the meniscus and glassy slag tends to fracture near mold exit. Medium casting speed may be the safest to avoid slag fracture due to its having the lowest critical lubrication consumption rate. The high measured friction force in operating casters could be due to three sources: an intermittent moving solid slag layer, excessive mold taper or mold misalignment.

I. INTRODUCTION

Many phenomena in continuous casting, including the formation of surface defects, are greatly affected by heat transfer in the mold[1-5]. The interfacial slag layer(s) between the solidifying steel shell and the mold wall dominates the resistance to heat removal and thus controls mold heat transfer in powder casting[6-8]. Surface defects, such as longitudinal cracks and star cracks have been attributed to variation of slag lubrication[9, 10]. High meniscus heat transfer and variation in meniscus heat transfer correlate with increased surface or subsurface defects [9, 11, 12], but the reasons are not understood. Thus, improved understanding of slag layer behavior is important for steel quality.

In continuous casting, mold powder is added to the free surface of the liquid steel. It sinters and melts, spreading over the liquid steel surface according to the steel surface contour and flow pattern[13]. During each oscillation stroke, liquid slag is pumped from the meniscus into the gap between the steel shell and the mold wall, where it acts as a lubricant[14, 15], so long as it remains liquid. A solid slag layer forms against the mold wall. Its thickness increases greatly just above the meniscus, where it is called the slag rim. Depending on the composition and cooling rate of the mold slag, the microstructure of the multiple layers that form may be glassy, crystalline or mixtures of both[16, 17]. Figure 1 shows a typical schematic of this region of the continuous casting process.

A substantial fraction of the slag consumed in the mold is entrapped in oscillation marks moving down at the casting speed. When a solid layer stably attaches to the mold wall, the remaining slag consumed is from the flowing liquid layer and is here called “lubrication consumption”.

Compared with oil lubrication, powder(/slag) lubrication leads to more uniform and usually lower heat transfer[5, 18]. The heat flux across the interfacial gap depends on the slag layer thermal properties[19-21] and thickness[8, 22], which is affected by slag properties such as melting, crystallization behavior and temperature dependent viscosity[23, 24]. It is reported that slag conductivity dominates heat transfer across the crystalline layer, although radiation is very important across glassy and liquid layers[21]. High solidification temperature crystalline slag usually reduces mold heat transfer[24]. This is likely due to the lower conductivity of crystalline slag[25] and the thicker solid slag layer that accompanies the higher solidification temperatures.

The hydrostatic or "ferrostatic" pressure of the molten steel pushes the unsupported steel shell against the mold walls, causing friction between the steel shell and the oscillating mold wall. At the corners, the shell may shrink away to form a gap, so friction there is often negligible. However, friction at the bottom of the narrow faces becomes a significant source of friction if excessive taper squeezes the wide face shell. Finally, misalignment of the mold and strand can cause friction, especially if the stroke is large. It has been proposed that friction may impede increased casting speed[26]. This work also investigates friction as a cause of fracturing of the solidified slag layer that produces local heat flux variation. The accompanying temperature and stress variations in the steel shell could lead to quality problems, such as shear tearing, sticking and even breakouts[27-29]. Ozgu[30] and Geist[31] both report "saw-tooth" shape temperature fluctuation low in the mold, which suggests solid slag layer fracture and sheeting from the mold wall[32]. Currently mold friction measurements are evaluated mainly as a means to detect problems with the oscillation system, such as mold misalignment. If the friction signal can be better understood, friction monitoring could be used to identify the status of mold lubrication to predict surface defects[33] and to help prevent breakouts[34].

Figure 2(a) shows a 20cm long piece of slag film taken from the corner of an operating caster mold. Many researchers believe that a glassy slag layer forms against the mold wall due to high cooling rates during initial contact of the molten slag with the water-cooled copper mold. A liquid layer is present when the shell surface temperature is higher than the slag solidification temperature. Between these two layers, a crystalline layer is expected, according to the time-temperature transformation (TTT) diagram, which has been measured recently in controlled laboratory conditions[35, 36]. However, slag film samples taken from the mold wall usually show a different microstructure: a crystalline layer toward the mold side and glassy layer on the shell side[25, 32], as shown in Fig. 2(b). Perhaps the glassy layer devitrifies during the long period when solid layer attaches to the mold wall[32] and perhaps the steel-side glassy layer forms from air-quenching the liquid slag while obtaining the sample.

To understand and quantify these phenomena, it is necessary to simulate transport and stress in the molten and re-solidified slag layers in the shell-mold gap. Models of steel solidification and heat transfer in continuous casting are reviewed previously[37]. Only a few models have detailed treatment of the interfacial layers. Of these, most assume a linear velocity distribution through the liquid film thickness[21, 26, 38, 39]. Several previous models have attempted to quantify gap flow by solving a Navier-Stokes equation[28, 40-49]. In these models, the slag layer thickness either is an input constant[40, 42, 45, 47, 48], an input function[43, 49] or assumed to equal the shrinkage of the steel shell[28, 41, 44, 46]. This ignores important phenomena such as ferrostatic pressure. Most previous models assume constant slag viscosity in the gap[40, 42, 43, 45, 49, 50], which is contrary to the tremendous temperature dependency reported in measurements[51-54] and high temperature gradient across the gap. Some researchers fit slag viscosity to a simple inverse function of temperature[28] or an Arrhenius equation[41, 44, 47, 51]. However, the slag viscosity is only

measured above the slag liquidus and is much lower on the mold side. Seldom have models discussed the effect of oscillation marks on lubrication and consumption. Moreover, no previous model describes solid layer fracture and sliding behavior of the slag layers. Thus, a more comprehensive model of interfacial gap lubrication and heat transfer was developed in this work.

II. INTERFACE MODEL DESCRIPTION AND VALIDATION

The present work models heat transfer, liquid flow and friction in the interfacial slag layers during an oscillation cycle. An analytical solution of the 2D momentum equation is derived for a temperature-dependent viscosity in the liquid slag layer. The model is validated through comparison with a numerical solution, based on heat transfer calculated for typical casting conditions. Shear stress in the liquid slag layer is based on the velocity gradient and liquid viscosity. Next, axial stress and friction in the solid slag layer is obtained by solving a force balance equation. This model is validated using ANSYS. Finally, the program with combined heat transfer, liquid flow and solid friction models, CON1D, is applied to predict typical behavior and critical conditions for fracture and sliding of the interfacial slag layers.

A. *Heat Transfer Model*

A simple but comprehensive model of heat transfer and solidification in continuous cast steel, CON1D, is used for the current study. The model includes a 1-D transient finite-difference calculation of heat conduction in the solidifying steel shell coupled with 2-D steady-state heat conduction in the mold wall. It features a detailed treatment of the interfacial gap between the shell and the mold, including mass and momentum balances on the slag layers and the effect of oscillation marks. Details of this model are presented elsewhere[37].

B. *Liquid Slag Layer Flow Model*

For simplicity, the slag is treated as two layers each with variable thickness in the vertical (z-) direction: a rigid solid layer and a laminar liquid layer with temperature dependent viscosity. A schematic profile of the mold, slag and steel shell velocities is shown in Fig. 3 for the case when the solid slag layer is stuck to the mold wall so its average downward velocity, V_s, is zero. The steel shell moves downward at the casting speed V_c, and the mold oscillates in the vertical direction with the sinusoidal displacement function:

$$Z_m = Z_0 + \frac{s}{2}\sin\left(2\pi ft\right) \qquad [1]$$

A mass balance on the liquid slag layer gives the following continuity equation, assuming incompressible flow, constant density and identical behavior within any vertical slice, so velocity across the slab width, V_y is zero:

$$\frac{\partial V_x}{\partial x} + \frac{\partial V_z}{\partial z} = 0 \qquad [2]$$

The following Navier-Stokes equation characterizes the laminar viscous flow of liquid slag vertically within the gap:

$$\begin{aligned} &\rho_{slag} \cdot \left(\frac{\partial V_z}{\partial t} + V_x \cdot \frac{\partial V_z}{\partial x} + V_y \cdot \frac{\partial V_z}{\partial y} + V_z \cdot \frac{\partial V_z}{\partial z} \right) \\ &= -\frac{\partial P}{\partial z} + \frac{\partial \tau_{xz}}{\partial x} + \frac{\partial \tau_{yz}}{\partial y} + \frac{\partial \tau_{zz}}{\partial z} + \rho_{slag} g \end{aligned} \qquad [3]$$

In the horizontal direction, the internal pressure, P, is assumed to equal the ferrostatic pressure, which is transmitted directly across the steel shell, so:

$$\frac{\partial P}{\partial z} = \rho_{steel} g \qquad [4]$$

This is reasonable everywhere except near the corners that support themselves and near the meniscus where pressure fluctuates. Thus, this model is appropriate within most of the gap over the unsupported wide faces of slab casting.

In Eq.[3], $V_y \frac{\partial V_z}{\partial y}$ and $\frac{\partial \tau_{yz}}{\partial y}$ can be neglected because V_y=0. The three terms $\rho_{slag} V_x \frac{\partial V_z}{\partial y}$, $\rho_{slag} V_z \frac{\partial V_z}{\partial z}$ and $\frac{\partial \tau_{zz}}{\partial z}$ are shown to be negligible in the next section for typical continuous casting conditions. Thus Eq.[3] simplifies to the following as gravity and downward viscous drag by the steel shell must balance the upward squeezing from the ferrostatic pressure:

$$\rho_{slag} \cdot \frac{\partial V_z}{\partial t} = \frac{\partial \tau_{xz}}{\partial x} + \left(\rho_{slag} - \rho_{steel} \right) g \qquad [5]$$

Shear stress in the liquid slag layer depends on the velocity gradient at each point across the channel:

$$\tau_{xz} = \mu \frac{\partial V_z}{\partial x} \qquad [6]$$

The temperature dependent viscosity of the liquid slag is fit to a simple power-law relation, which better represents low-temperature high-viscosity behavior than a simple Arrhenius equation[51]:

$$\mu = \mu_s \left(\frac{T_s^{'} - T_{fsol}}{T - T_{fsol}} \right)^n \qquad [7]$$

Assuming that temperature across the liquid slag layer thickness is linear gives:

$$T = \frac{x}{d_l} \left(T_s^{'} - T_{fsol} \right) + \ T_{fsol} \qquad [8]$$

Substituting Eq.[8] into Eq.[7] and replacing the viscosity term in Eq.[6] with this position dependent viscosity yields:

$$\tau_{xz} = \mu_s \frac{d_l^n}{x^n} \frac{\partial V_z}{\partial x} \qquad [9]$$

Differentiating Eq.[9] and substituting into Eq.[5], yields the following momentum equation, governing the velocity distribution in the liquid film:

$$\rho_{slag} \frac{\partial V_z}{\partial t} = \mu_s \frac{d_l^n}{x^n} \frac{\partial^2 V_z}{\partial x^2} - \mu_s \frac{n d_l^n}{x^{n+1}} \frac{\partial V_z}{\partial x} + \left(\rho_{slag} - \rho_{steel}\right) g \qquad [10]$$

Differentiating Eq.[1] to get mold velocity V_m, and assuming the solid slag is attached to the mold wall, the boundary conditions for the liquid slag layer model, Eq.[10], are:

$$\text{solid/liquid slag layer interface: } V_z\Big|_{x=0} = V_s = V_m = \pi sf \cdot \cos\left(2\pi ft\right) \qquad [11]$$

$$\text{liquid slag/steel shell interface: } V_z\Big|_{x=d_l} = V_c \qquad [12]$$

Neglecting $\frac{\partial V_z}{\partial t}$ and applying the boundary conditions Eqs.[11] and [12], Eq.[10] can be integrated to obtain the following "pseudo-transient" analytical solution:

$$V_z = \frac{-\left(\rho_{slag} - \rho_{steel}\right) g x^{n+2}}{\mu_s \left(n+2\right) d_l^n} + \left(\frac{\left(V_c - V_s\right)}{d_l} + \frac{\left(\rho_{slag} - \rho_{steel}\right) g d_l}{\mu_s \left(n+2\right)} \right) \frac{x^{n+1}}{d_l^n} + V_s \qquad [13]$$

C. *Liquid Slag Layer Flow Model Validation*

To check the validity of the assumptions made to obtain Eq.[13], a fully transient numerical solution was obtained using an explicit finite-difference discretization of Eq.[10] with a central difference scheme:

$$V_z^{i(t+\Delta t)} = V_z^{i(t)} + \frac{\Delta t}{\rho_{slag}} \left(\mu_s \frac{d_l^n}{x^n} \frac{V_z^{i+1(t)} - 2V_z^{i(t)} + V_z^{i-1(t)}}{\Delta x^2} - \mu_s \frac{n d_l^n}{x^{n+1}} \frac{V_z^{i+1(t)} - V_z^{i-1(t)}}{\Delta x} + \left(\rho_{slag} - \rho_{steel}\right) g \right) \qquad [14]$$

A MATLAB[55] program was coded to solve this equation with boundary conditions Eqs.[11] and [12] at different z-distances. Table II gives the parameters of 4 cases used in the MATLAB

program. Cases (a)-(b) are based on heat transfer results for typical casting conditions as shown in Table I; and Cases (c)-(d) use an extremely thick liquid layer (2mm) from Chavez's work[47]. Discretizing the continuity equation Eq.[2] and processing the results at different z-distances (specifically z=53mm and z=54mm for case (b)) allow computations of the other terms in Eq.[3]. Table III shows values of the different terms in Eq.[3] for case (b) at t=0.18s, x=0.16mm. Note that $\rho_{slag} V_x \frac{\partial V_z}{\partial x}$, $\rho_{slag} V_z \frac{\partial V_z}{\partial z}$ and $\frac{\partial \tau_{zz}}{\partial z}$ are negligible compared to the other terms. Also note that the transient term $\rho_{slag} \frac{\partial V_z}{\partial t}$ contributes less than 1.5%, so can justifiably be neglected too.

Figure 4 shows typical velocity profiles computed with these models. For constant viscosity and a thin liquid layer, Fig. 4(a), the velocity profiles are linear. Otherwise, nonlinearity is significant. Figure 4 also compares the numerical solution and the pseudo-transient analytical solution. It shows that the transient effect is negligible for a film thickness of 0.2mm. Even for an extreme case, 2mm thick liquid film, Fig. 4(c), (d), the maximum transient effect is barely perceptible. Therefore the pseudo-transient analytical solution to the liquid slag layer flow equation, Eq.[13] is a reasonable approximation of the full transient solution.

Substituting Eq.[13] into Eq.[9] gives:

$$\tau_{xz} = \frac{(n+1)\mu_s (V_c - V_s)}{d_l} + \frac{(\rho_{slag} - \rho_{steel}) g ((n+1) d_l - (n+2) x)}{n+2} \qquad [15]$$

Evaluating Eq.[15] at x=d_l gives the shear stress at the slag/steel interface when a liquid slag layer is present:

$$\tau_{liquid\ flux/steel} = \mu_s \frac{(n+1)(V_c - V_s)}{d_l} - \frac{(\rho_{slag} - \rho_{steel}) g d_l}{(n+2)} \qquad [16]$$

D. *Solid Slag Layer Stress Model*

Near the meniscus, the solid slag layer attaches to the mold wall and oscillates with the mold. However, if the solid slag layer breaks, and where it breaks, could greatly affect heat transfer across the gap. A stress model is developed to investigate force balances and possible fracture in the solid slag layer.

The equilibrium force balance in the axial z-direction is:

$$\frac{\partial \tau_{xz}}{\partial x} + \frac{\partial \sigma_z}{\partial z} + F_z = 0 \qquad [17]$$

Knowing that body forces F_z are negligible in the solid layer, Fig. 5 illustrates the force balance in a solid slag layer discretization element cut from Fig. 1 for four typical cases. Evaluating τ_{xz} in Eq.[15] at x=0 gives the shear stress boundary condition at the interface between the liquid and solid slag layers:

$$\tau_{s/l} = \mu_s \frac{(n+1)\left(V_c - V_s(t)\right)}{d_l} + \frac{(n+1)}{(n+2)}\left(\rho_{slag} - \rho_{steel}\right) g d_l \qquad [18]$$

Note that this shear stress varies greatly during the oscillation cycle.

The maximum shear stress transmitted to the mold by Coulomb friction with the solid slag layer, due to relative motion of the mold and shell is:

$$\tau_{max} = \phi_{static} \cdot \sigma_x \qquad [19]$$

The normal stress, σ_x, comes from the liquid steel ferrostatic pressure and the liquid slag pool above the meniscus, which generates a tiny additional head:

$$\sigma_x = -\left(\rho_{slag} g h_0 + \rho_{steel} g z\right) \qquad [20]$$

Shear stress must be continuous across the gap, including both the boundaries at the mold and steel shell surfaces. When the liquid layer/steel interface shear stress is smaller than the maximum solid contact shear stress, then the friction force drops to match it, as shown in Fig.

5(a). In this "liquid shear stress limited" case, Fig. 5(a), the friction force is less than the maximum possible static friction given in Eq.[19]. Ferrostatic pressure then generates axial stress σ_z in the solid layer that is compressive:

$$\sigma_z = -\frac{\upsilon}{1-\upsilon}\sigma_x \qquad [21]$$

so *xz*-shear stress at the mold side can be calculated from Eqs.[17, 20, and 21] as follows:

$$\tau_{mold} = -\int_{x=0}^{d_s} d\sigma_z / dz \cdot dx + \tau_{s/l} = \frac{\upsilon}{1-\upsilon}\rho_{steel} g d_s + \tau_{s/l} \qquad [22]$$

Alternatively, if the liquid layer shear stress is larger than the maximum static friction, $\tau_{mold} = \tau_{max}$, then axial stress develops in the solid layer to compensate. In order to satisfy the force balance Eq.[17]:

$$d\sigma_z = -d\tau_{xz} \cdot dz / dx \qquad [23]$$

Discretizing Eq.[23] axially, and integrating across the thickness, the axial stress in the solid slag layer at $z+\Delta z$ is:

$$\sigma_{z+\Delta z} = \sigma_z - \frac{\tau_{max} - \tau_{s/l}}{d_s}\Delta z \qquad [24]$$

Specifically, axial stress is tensile during the up-stroke and compressive in the down-stroke for this "mold friction limited" case shown in Fig. 5(b). Furthermore, the axial tension accumulates over successive slices of the solid slag layer. The shear stress transmitted to the mold wall is the minimum of the maximum static friction stress and the solid/liquid interface stress:

$$\tau_{mold} = min\left(\frac{\upsilon}{1-\upsilon}\rho_{steel} g d_s + \tau_{s/l}, \tau_{max}\right) \qquad [25]$$

E. *Solid Slag Layer Stress Model Validation*

To validate the stress model of the solid slag layer, a simplified case was solved using elastic finite-element stress analysis with ANSYS[56]. Figure 6 shows the ANSYS model domain and mesh. The boundary condition at the mold side had displacements fixed to zero and at the liquid side was normal ferrostatic pressure, σ_x, from Eq.[20] and tangential shear stress, $\tau_{s/l}$ (from CON1D). Table I gives the input conditions and simulation parameters used in CON1D. Figure 7 compares the stress results from ANSYS and CON1D using Eqs.[24] and [25]. The CON1D model matches ANSYS except within 10mm near mold exit, where the real axial stress must quickly tend to zero (to match ambient atmospheric pressure).

F. *Solid Slag Layer Fracture Model*

If the axial stress exceeds the fracture strength, the solid slag layer will break, and be dragged down the mold wall. The shear stress on the mold/slag interface for this condition is:

$$\tau_{mold} = \phi_{moving} \cdot \sigma_x \qquad [26]$$

Substituting Eqs. [18] and [26] into Eq.[22] can solve for the solid layer velocity V_s after it detaches from the mold wall. Fracture and sliding of the solid slag layer tend to create a gap between the upper attached solid layer and the lower moving layer. This gap may re-fill with liquid slag, and the solid layer might re-attach to the mold wall when the instantaneous velocity of the oscillating mold wall equals the moving solid slag layer velocity. The time for the liquid slag to fill the gap and the solid slag to re-attach depends on the slag consumption rate and liquid slag fluidity. The fracture and filling process requires extra slag consumption, which decreases the liquid layer thickness and increases shear stress(/friction) for the whole mold.

G. *Mold Friction*

The friction measured in operating casting molds may come from mold/slag contact, excessive taper, misalignment or a combination of the three.

(1) Slag layer friction Previous research has suggested that friction against the slag layer is important[57]. The liquid slag-layer flow model and solid slag-layer stress model described in this work give the shear stress on the mold wall, τ_{mold}, due to mold/slag contact. Integrating the shear stress over the mold face gives the total friction force due to contact between the mold and slag layers:

$$F_{contact} = \int_0^{Z_{mold}} \tau_{mold} \cdot 2(W+N) \cdot dz \qquad [27]$$

where, Z_{mold}: working mold length; W: slab width; N: slab thickness.

This model has been incorporated into CON1D, and is used for the study described in sections III and IV.

(2) Excessive taper If the solid slag layer remains attached to the mold wall all the way down the mold, there will be a continuous, thick liquid slag layer (to provide slag consumption) and a thick solid slag layer, leading to low heat transfer across the mold/shell gap. Then the shell will have relatively high surface temperature and small shrinkage. In this case, excessive narrow face taper may squeeze the steel shell and therefore lead to increased friction. The maximum force from squeezing the shell occurs if the shell buckles, leading to longitudinal surface depressions, such as off-corner gutter in extreme cases[13], as shown in Fig. 8. Applying the Eular critical buckling load equation with rigid ends yields an estimate of the normal stress on the mold wall, F_{cr}:

$$F_{cr} = \frac{4\pi^2 EI}{L_{eff}^{\ 2}} = \frac{4\pi^2 E}{L_{eff}^{\ 2}} \frac{b^3 h}{12} \qquad [28]$$

Where, b is the shell thickness, h is the vertical contact length along the narrow face, L_{eff} is the unsupported shell width across the wide face from the corner and E is the effective elastic modulus of the hot steel shell. So the friction due to buckling for each narrow face is:

$$F_{excessive\ taper} = 2\phi_{static} \cdot F_{cr} \quad [29]$$

(3) Misalignment friction Misalignment of the mold and strand is another important potential cause of friction. The friction force during each oscillation cycle is inferred from the difference between the force transducer measurements with and without molten steel in the mold[58]. Currently, such friction signals can be used to monitor and detect misalignment problems in operating casters.

III. EXAMPLE APPLICATION

The CON1D model is first used to simulate behavior for the typical casting conditions listed in Table I. During casting, mold slag may absorb reoxidation products such as alumina. This changes the slag composition and its properties. Alumina tends to decrease slag basicity[52], which decreases the crystallization temperature[52, 59, 60] and increases viscosity at high temperature[52, 59-61]. This makes the slag easier to be glassy[59, 62]. Figure 9 shows the viscosity curves vs. temperature assumed for three slags, which were chosen to match with slag viscosity data measured by Lanyi[52]. The typical continuous casting Slag A might be crystalline or glassy (Slag A2 in Lanyi[52]); Slag C is readily crystalline (Slag A6 in Lanyi[52]). Slag G is Slag C with 25% additional alumina, which has a high tendency to be glassy[52]. The composition and properties of these three slags are listed in Table IV.

Computation of both heat transfer and friction depends greatly on the total consumption rate of slag into the gap, Q_{slag}(kg/m^2), which is an input parameter in this work. It is important to introduce the concept of "lubricating consumption rate": Q_{lub}, which is the slag consumption not carried inside the oscillation marks:

$$Q_{lub} = Q_{slag} - Q_{osc} \quad [30]$$

where, Q_{osc}: the consumption rate of slag carried within the filled oscillation marks is found from:

$$Q_{osc} = 0.5\rho \cdot d_{mark} \cdot w_{mark} / L_{pitch} \quad [31]$$

The liquid slag represented by Q_{lub} acts to lubricate the mold-shell interface and thereby lower friction. The CON1D model is run with different mold slags, consumption rates and casting speeds to study the effect of mold powder properties and oscillation practice. The related parameters are listed in Tables IV to VI.

A. *Typical Results*

Simulations were first run for typical low friction conditions, Case I (Table I), assuming that all solid slag is attached to the mold wall and constant lubrication consumption rate Q_{lub}, of 0.2kg/m^2. At 1.0m/min casting speed, total consumption rate, Q_{slag} is 0.41kg/m^2. Figure 10 shows typical results with Slag A. The mean heat flux in the mold is 1.24MW/m^2 and the shell thickness is 20.4mm at mold exit (based on a solid fraction of 0.3). A uniform liquid slag layer of 0.29mm is predicted, Fig. 10(d), while the solid layer continually increases down the mold. Such a thick solid layer could build up over time starting during initial mold filling with starter slag. Once it reaches steady state, it does not consume any new mold powder. Increasing casting speed is naturally predicted to raise heat flux but lower shell growth.

Figure 11 shows the cooling history of various points in the slag layer for Case I with Slags A and G. The superimposed TTT curve of a conventional industrial mold slag (7.9%Al_2O_3)[63] is used to estimate the onset of crystallization for Slag A. Figure 11(a) predicts crystallization in most of the slag layer (including the oscillation marks) except the very thin (0.2mm) layer adjacent to the mold wall, which is quenched rapidly and remains glassy. Extra alumina in the slag delays the onset of crystallization and increases the temperature range of crystallization, so

the TTT curve of a slag with 19.5% Al_2O_3[64] is used to estimate the onset of crystallization for Slag G. Figure 11(b) shows that no points within Slag G cross the TTT curve, so no crystalline phase is predicted. This agrees with the assumption that Slag G tends to be glassy.

Shear stress and axial stress along the solid slag layer was plotted in Fig. 7. It shows that the solid slag layer is in compression almost everywhere. Therefore the attached solid slag layer is stable and no fracture should occur. This can happen in practice, as evidenced by the recovery of a solid slag layer attached to the mold wall after one hour of casting, which contains trace elements only found in the starter slag (consumed in the first few minutes)[65, 66]. The accompanying stable, thick liquid layer ensures a very low friction force on the mold wall.

Figure 12(a) predicts the slag layer thicknesses of the glassy and crystalline slags, assuming the same consumption rate and other conditions (Table I). Glassy slag G is thinner due to its lower solidification temperature. Therefore it produces a slightly higher heat flux and lower shell temperature than the crystalline slag, as shown in Fig. 12(b)(c). If the lower consumption rate that generally accompanies higher viscosity slags in a real caster[67, 68] were taken into account, these differences would be even greater. In either case, this prediction matches well-known measured behavior[25, 68, 69].

Note that the crystalline slag is predicted to have lower friction on the mold wall, Fig. 12(d). This is mainly because of its lower viscosity gradient at high temperature (Fig. 9), which helps the solid crystalline layer to stay attached to the mold wall and prevent fracture.

B. *Critical Slag Consumption Rate*

Lower slag consumption rate, Q_{lub}, leads to higher shear stress at the liquid/solid slag interface. If friction on the mold side cannot balance the shear stress along the solid/liquid interface, axial tensile stress must build up in the solid slag layer to compensate. When axial

stress in the solid slag exceeds the slag fracture strength, the solid slag breaks and is dragged down the mold wall. The critical consumption rate is the minimum consumption rate needed to keep solid slag attached to the mold wall without breaking or sliding. In order to find it, the complete CON1D model was run several times with different consumption rates, Case II, assuming slag fracture strength of 80MPa[70]. Figure 13 shows the axial stress and shear stress distribution of slags A and G along the mold wall at their corresponding critical consumption rates. It shows that tensile axial stress accumulates in the solid slag only when liquid shear stress exceeds maximum static solid friction. In each case, fracture is predicted during the upstroke when axial stress just exceeds the slag fracture strength. All stresses are compressive during the down stroke.

Slag G has 60% larger critical lubricating consumption rate, Q_{lub}, 0.12kg/m^2 than Slag A, 0.075kg/m^2. Slag C has similar behavior to Slag A, but with an even lower critical Q_{lub}, 0.05kg/m^2. It confirms the general observations that crystalline slags are more stable than glassy slags. Combined with their thicker layer and lower heat flux, this may explain why such crystalline slags are better for depression and crack sensitive steel grades[7, 69].

Another important difference between Slag A/C and G is the position of slag fracture. As consumption rate lowers, the glassy slag drops below the critical consumption rate first and fractures first near the mold exit. For crystalline slags A and C, the solid slag layer fractures within 100mm near the meniscus. These results show that the sharpness of the slag viscosity increase near the solidification temperature is more important than the popular slag property, slag viscosity at 1300^{o}C.

Figure 14 shows the heat flux and mold temperature of these two critical cases. Relative to Case I, very high heat flux is predicted near the meniscus. This is also indicated by the high mold

temperature at that region. This also implies that in a real caster, if an abnormal high mold temperature is observed near the meniscus, it may due to a temporary consumption rate drop regardless of slag type. This should also correlate with solid slag breaking and moving down the mold wall. Slag fracture in turn will cause temporary gaps, heat flux drops, and thermal stresses in the shell. The phenomena of high meniscus heat flux and high variations are known to correlate with strand defects[11, 12], which is consistent with the model prediction here.

C. *Mold Friction*

(1) Attached slag layer When casting with a stable conventional consumption rate (Q_{slag}=0.41kg/m^2), the model predicts a stable solid slag layer and a very low friction force. For the cases studied here, the mold wall shear stress amplitude is 0.85MPa for slag A, and 2.52MPa for slag G, which are far lower than reported measured friction data[71]. The high friction force measured in operating casters likely comes from three possible causes: a moving solid slag layer, excessive taper or misalignment.

(2) Moving solid slag layer If the liquid slag level at the meniscus varies, it cannot keep a steady flow into the mold/strand gap even if the mold taper and alignment are reasonable and do not contribute to friction. The solid slag layer may break and move along the mold wall, accounting for part of the slag consumption. For a given consumption rate, the liquid slag layer is thinner when the solid layer moves. This leads to higher heat flux and higher friction and therefore perpetuates the slag fracture and motion. The fracture position predicted for slag A (Case II with critical consumption rate) is near the meniscus. Thus, the low viscosity liquid layer may quickly fill in the gap due to facture, and the solid slag layer might reattach to the mold wall until the next fracture. For slag G, if the consumption temporarily drops lower than the critical consumption rate, the solid slag layer fracture will occur further above mold exit.

To model a moving solid slag layer, its average velocity is simply assumed to be some small constant percentage of the casting speed, v_f. In case III, assuming $v_f \approx 5\%$ produces total friction force predictions within the measured range of 15~23kPa[71]. Note the average "moving" solid slag layer velocity is actually the time average of a highly transient process, calculated with an intermittent procedure of solid layer fracture, movement and re-attachment. Most of the time, the solid layer still sticks to the mold wall, so the shear stress can still be calculated based on liquid layer friction and the maximum static friction between mold and solid layer. Figure 15 shows that both liquid and solid moving layers are thinner than for the attached case. In particular, the liquid slag layer gets thinner with distance down the mold and nearly runs out by mold exit. This increases friction greatly.

(3) Friction variation during an oscillation cycle Figure 16(a) shows the mold velocity and casting speed profile during half of one oscillation cycle. It shows that at one instant, 0.24second, the mold velocity equals the casting speed, so there is no shear stress. After that time, the mold moves down faster than the shell during the period of "negative strip". Thus, the stress acting on the slag layer shifts from tension to compression during that instant. Figures 16 also shows that the shear stress on the mold wall with a "moving" solid slag layer, (c), is much higher than with an attached layer, (b). Shear stress increases with distance along the mold length, and the transition from tension to compression becomes sharper for a moving layer. In the upper mold, liquid slag controls the friction between mold and shell, so the shear stress is nearly sinusoidal. In the lower mold region, the solid slag layer controls friction and the shear stress profile tends toward a square wave.

Figure 17 shows the shear stress down the mold at different times during the oscillation cycle. For all times, there is a transition from curved to straight, where liquid slag layer control

transfers to solid slag layer control. The "average" is the mean of the absolute values of all the shear stresses over the whole oscillation cycle, and is very near to the curve when V_m is zero. This means that the average friction force can be estimated with a simple static mold model. Integrating the shear stress over each mold face at each instant gives the total friction force history during each oscillation cycle, as shown in Fig. 18 for different cases.

(4) Total mold friction Figure 18 shows that the friction due to shear stress is very small if the solid slag layer is attached and there are no other sources of friction. Friction with an intermittent attached solid layer is 10X larger and has a sharper transition from tension to compression. Another possible cause of high friction may be squeezing of the steel shell due to excessive narrow face taper. This is most likely when the shell temperature is high and shrinkage is small at high casting speed. A rough estimation of the magnitude of this friction is 15kN on each narrow face, based on Eqs.[28],[29], assuming buckling happens over the last 10mm (h=10mm) near mold exit, shell thickness b=20mm, L_{eff}=600mm, E=25GPa at 1100^{o}C. This corresponds to an average friction stress over a 800mm long 230mm thick and 1500mm wide slab mold of 10kPa, which is similar to measured data[71]. Figure 18 shows that the friction force during an oscillation cycle for excessive taper can be identified by its almost-square shape. In contrast, liquid slag lubrication produces a smooth curve with a very gradual transition. Thus the lubrication/friction state of the mold can be identified from the shape of the friction force curve during an oscillation cycle in addition to its magnitude. Misalignment friction curves are expected to be curved according to gradual changes in its extent during the cycle.

IV. CONSUMPTION AND CASTING SPEED STUDY

A. *Effect of Slag Properties on Critical Consumption Rate*

The most important parameter affecting slag shear stress and fracture was found to be the liquid slag consumption rate. So long as consumption rate exceeds a minimum critical rate, the slag will not fracture. A parametric study was conducted on the minimum critical consumption to keep a stable attached solid slag layer. Doubling the fracture strength of the crystalline mold slag allows the critical Q_{lub} for slag A to decrease by only 7% and delays the fracture position from 60mm to 100mm below the meniscus. The fracture strength has even less effect for slag G. The effects of slag Poisson's ratio, liquid slag pool depth, and mold thickness on critical consumption rate were negligible.

Maintaining a high mold/slag friction coefficient is important to lowering the critical consumption. As shown in Fig. 19, especially for slag G, when the friction coefficient is lower than 0.15, the slag layer can fracture, even for a stable conventional consumption rate.

Oscillation marks act as an extra resistance layer between the liquid slag layer and the steel shell. Thus they slightly lower temperature in the liquid layer, which leads to higher viscosity liquid, higher shear stress, easier flux fracture and higher critical consumption. Specifically, 0.45mm*4.5mm oscillation marks cast at 1.0m/min increase Q_{lub} by 0.01kg/m^2 for both slags (15% for slag A and 9% for slag G) relative to cases with no oscillation marks

B. *Effect of Casting Speed on Critical Consumption Rate*

The influence of casting speed on mold friction and interface heat flux has been investigated in a parametric study. Based on Case I, the casting speed was varied from 1.0m/min to 5.0m/min. The stroke was fixed at 7.8mm, and oscillation frequency adjusted to keep a constant negative strip ratio of 0.3 and a constant pitch length of 12mm. Negative strip time

thereby decreases with increasing casting speed, so oscillation mark depth decreases[72]. The powder consumption rate thus decreases due to the shallower oscillation marks and higher oscillation frequency[73]. Oscillation mark depth becomes negligible when casting speed is greater than 2m/min. Table VI gives the mold oscillation parameters used. Those parameters are chosen based on some previous plant measurements of oscillation marks depth[72] and total mold powder consumption rate[11, 26, 74, 75] as shown in Figs. 20 and 21.

Figure 21 also compares measured consumption rates[11, 26, 74, 75] with critical consumption rates calculated in this study. Measured consumption rates exceed the critical rates, which indicates that slag fracture should be a rare transient event. If the total consumption rate can be steadily maintained, the strand should be well lubricated and a stable solid slag layer should remain attached to the mold. Figure 21 shows that measured consumption rates decrease with increasing casting speed. When there is significant consumption by the oscillation marks, Q_{osc}, the critical consumption also decreases with increasing casting speed. This is because oscillation mark depth decreases, carries less slag and increases the lubrication consumption component, thus helping to keep the solid layer attached to the mold wall as explained above. However, at higher casting speed (>2m/min), when the oscillation mark effect is negligible, the critical consumption rate increases slightly with casting speed.

Figure 22 shows two opposing effects of casting speed on solid slag fracture, excluding oscillation marks and their effects. Increasing casting speed increases the velocity difference between mold and shell, which tends to increase friction. It also increases shell surface temperature, which tends to decrease slag viscosity and friction. For slag A, the first effect prevails, so the slag always fails near the meniscus and higher casting speed is more dangerous to slag fracture. To be specific, increasing V_c from 1.0m/min to 2.0 m/min, requires the critical

Q_{lub} to increase by 25%. Also, the fracture position occurs closer to the meniscus (moving from 60mm to 30mm). When the critical fracture position is near to the mold exit, such as slag G at less than 3.0m/min, the effect of higher surface temperature predominates, so higher casting speed helps to avoid slag fracture, as shown in Fig. 22(b). Thus, increasing casting speed from 1.0m/min to 2.0m/min decreases critical Q_{lub} by 8%. However, further increasing casting speed above 3.0m/min causes the critical fracture position to move to near the meniscus, and increases the critical Q_{lub} as for slag A.

Note that the minimum critical consumption rate occurs at intermediate speed (~2m/min) for the conditions of this study, which is the safest speed for slag layer stability. Measured consumption rates exceed the calculated critical consumption rates by the largest factor (~3X) for this intermediate speed. Safety margins are less at both lower speed and higher speed. At very high speed, ~5m/min, measured consumptions approach critical levels. This indicates that solid slag layer stability becomes a general problem at high speed (unless consumption or another condition assumed here is changed).

Figure 23 compares the average heat flux with measured and fitted data[76-79]. Average mold heat flux increases with higher casting speed, with lower consumption rate or with a moving solid slag layer. Note that the average heat flux of the cases with moving slag or with critical consumption rate (just about to move) almost hit the upper bound of measurements. High and variable heat flux is another indication of slag layer fracture.

C. *Effect of Casting Speed on Friction Stress*

Finally, CON1D was run with a detached solid slag layer assumed to be moving at an average velocity of 5% of the casting speed (Case III). The lubrication consumption rate Q_{lub} was assumed to remain the same, 0.2kg/m^2, for all cases. The solid friction force with moving slag is

much higher than for the attached cases, and increases with decreasing casting speed. These predictions compare with measured data[71], as shown in Fig. 24. The agreement at lower casting speed is consistent with the prediction that solid slag fracture and movement increases at lower speed. The high friction at high speed might be due to other friction sources such as excessive mold taper. Also note that for the same average solid layer moving speed, glassy slag has higher friction than crystalline slag. It is interesting speculate that the drop in friction at intermediate speed might correspond to the minimum in critical consumption rate and maximum safety factor predicted in this work. It implies that solid slag layer fracture may be more likely at both low and high casting speed, perhaps increasing the higher average solid layer moving speed, which would increase friction. This is consistent with measurements in Fig. 24.

V. CONCLUSIONS

Analytical transient models of liquid slag flow and solid slag stress are developed and incorporated into a finite-difference model of heat transfer in the shell and mold (CON1D). All three models have been validated extensively with plants measurements. They are applied to study the effect of casting speed and mold powder properties on slag layer behavior between the oscillating mold wall and solidifying steel shell. Specific conclusions are:

1. Solid slag tends to remain attached to the mold wall, especially near the meniscus. When friction on the mold side cannot compensate the shear stress on the slag solid/liquid interface, axial stress builds up in the solid slag layer. If the powder consumption rate drops below a critical level, the axial stress can exceed the slag fracture strength, so the solid slag breaks and moves down the mold wall.
2. Crystalline slag with higher solidification temperature has a thick solid slag layer so lowers heat transfer across the mold/shell gap and increases shell surface temperature.

3. The slag temperature-viscosity curve determines the shear stress along the mold wall and affects both the critical consumption rate and possible slag fracture position. Crystalline slag (having a sharp viscosity transition) tends to fracture near the meniscus, but not easily (lower critical Q_{lub}). Glassy slag (having a gradual viscosity rise at lower temperature) tends to fracture near mold exit, easily (higher critical Q_{lub}). Increasing slag solidification temperature and decreasing high-temperature viscosity (such as occurs with high basicity slag) tends to lower critical Q_{lub} and make it less easy to fracture.
4. The following variables lower axial stress in the solid slag layer, critical Q_{lub}, and the likelihood of slag fracture.
    - Increasing friction coefficient helps by encouraging the solid slag to stay attached to the mold wall.
    - Smaller oscillation marks lower gap friction and lower the danger of slag fracture.
    - Decreasing casting speed lowers critical Q_{lub} and the danger of slag fracture at the meniscus, such as for slag A and for slag G cast at high speed.
    - Increasing casting speed is safer for avoiding slag fracture near mold exit, such as for slag G cast at low speed.
    - Increasing slag fracture strength helps slightly.
5. Liquid slag layer lubrication indicates a stable attached solid slag layer and can be recognized by very low mold shear stress (~1kPa) with a sinusoidal variation over each oscillation cycle.
6. The top half of the mold has negligible friction against the steel shell, as the liquid slag layer minimizes it. Solid slag friction begins just before the liquid slag runs out, lower down the mold. Increasing the fraction of the mold with solid slag friction can be identified

by higher total mold friction and a sharper square wave shape of the friction curve over each cycle

7. The high friction (10~20kPa) measured in real casters might be due to any of three sources: an intermittent moving slag layer, excessive taper or mold misalignment. At low casting speed, the critical consumption rate is high, so variations in slag consumption at the meniscus can easily lead to solid slag layer fracture and movement. At high casting speed, excessive taper and mold misalignment likely increase friction problems.

NOMENCLATURE*

d_l/d_s liquid/solid slag film thickness (mm)

T_s steel surface temperature (at oscillation mark root)(^{o}C)

T_s' liquid slag layer hot side temperature (^{o}C)

V_m mold velocity (m/s)

x shell thickness direction, distance from the mold wall (m)

z casting direction, distance below the meniscus (m)

* Other symbols are defined in Table I

μ_s slag viscosity at hot side of liquid slag layer (Pa s)

σ_x normal stress on solid slag layer (Pa)

σ_z axial stress in solid slag layer (Pa)

τ_{max} maximum static shear stress on mold wall (Pa)

τ_{mold} shear stress on mold wall(Pa)

$\tau_{s/l}$ shear stress on slag solid /liquid interface (Pa)

ACKNOWLEDGEMENTS

The authors would like to thank the Continuous Casting Consortium of the University of Illinois and the National Science Foundation (Grant DMI-01-15486) for financial support.

REFERENCES

1. A.W.D. Hills: "Simplified Theoretical Treatment for the Transfer of Heat in Continuous-casting Machine Moulds", *Journal of the iron and steel institute,* 1965, pp. 18-26.

2. W.R. Irving: *Continuous Casting of Steel*, The Institute of Materials, London, 1993.

3. P.J. Zasowski and D.J. Sosinksy: "Control of Heat Removal in the Continuous Casting Mould", *Steelmaking Conference Proceedings*, (Detroit, Michigan, USA), 1990, vol. 73, pp. 253-59.

4. B.G. Thomas: "Mathematical Modeling of the Continuous Slab Casting Mold: a State of the Art Review", *1991 Steelmaking Conference*, 1991, pp. 69-82.

5. M.M. Wolf: "Mold heat transfer and lubrication control two major functions of caster productivity and quality assurance", in *Continuous Casting 1997*, vol. Volume 9: Initial Solidification and Strand Surface Quality of Peritectic Steels, Iron and Steel Society/AIME, 1997, pp. 211-22.

6. M.S. Jenkins: "Characterisation and Modification of the Heat Transfer Performance of Mold Powders", *Steelmaking Conference Proceedings*, (Nashville, Tennessee, USA), 1995, vol. 78, pp. 669-77.

7. J.W. Cho, T. Emi, H. Shibata and M. Suzuki: "Heat transfer across mold flux film in mold during initial solidification in continuous casting of steel", *ISIJ International (Japan),* 1998, vol. 38 (8), pp. 834-42.

8. K.C. Mills, S. Sridhar, A.S. Normanton and S.T. Mallaband: "Mould flux behaviour in continuous casting", *The Brimacombe Memorial Symposium*, (Vancouver, British Columbia, Canada), 2000, pp. 781-94.

9. T.J.H. Billany, A.S. Normanton, K.C. Mills and P. Grieveson: "Surface Cracking in Continuously Cast Producs", *Ironing and Steelmaking,* 1991, vol. 18 (6), pp. 403-10.

10. R. Bommaraju, R. Glennon and M. Frazee: "Analysis of the Cause and Prevention of Longitudinal Midface Cracks and Depressions on Continuously Cast Free-Machining Steel Blooms", *1st European Conference on Continuous Casting*, (Florence, Italy), 1991, vol. 1, pp. 1.599-1.610.

11. S. Hiraki, K. Nakajima, T. Murakami and T. Kanazawa: "Influence of mold heat fluxes on longitudinal surface cracks during high speed continuous casting of steel slab", *77th Steelmaking Conference*, (Chicago, IL, USA), 1994, vol. 77, pp. 397-403.

12. J. Konishi, M. Militzer, J.K. Brimacombe and I.V. Samarasekera: "Modeling the formation of longitudinal facial cracks during continuous casting of hypoperitectic steel", *Metallurgical and Materials Transactions B (USA),* 2002, vol. 33B (3), pp. 413-23B.

13. B.G. Thomas, A. Moitra and R. McDavid: "Simulation of longitudinal off-corner depressions in continuously cast steel slabs", *Iron and Steelmaker (USA),* 1996, vol. 23 (4), pp. 57-70.

14. E. Takeuchi and J.K. Brimacombe: "The Formation of Oscillation Marks in the Continuous Casting of Steel Slabs", *Metall. Trans. B,* 1984, vol. 15B (3), pp. 493-509.

15. T. Araki and M. Ikeda: "Optimization of mold oscillation for high speed casting--new criteria for mold oscillation", *Canadian Metallurgical Quarterly (Netherlands),* 1999, vol. 38 (5), pp. 295-300.

16. C.A. Pinheiro, I.V. Samarasekera and J.K. Brimacombe: "Mold Flux for Continuous Casting of Steel", *I&SM,* 1995, vol. 22 (2), pp. 37-39.

17. C. Orrling, S. Sridhar, Y. Kashiwaya and A.W. Cramb: "Crystallization phenomenon in slags", *58th Electric Furnace Conference and 17th Process Technology Conference*, (Orlando, FL, USA), 2000, pp. 211-21.

18. C.A.M. Pinheiro, I.V. Samarasekera and B.N. Walker: "Mould heat transfer and continously cast billet quality with mould flux lubrication", *Ironmaking and Steelmaking (UK),* 2000, vol. 27 (1), pp. 37-54.

19. B.I. Kubrik: "Effects of Thermal and Physical Properties of Slag and Coefficients of Thermal Conductivity of Mould Walls on Heat Transfer in Mould", *Steel USSR,* 1987, vol. 17 (12), pp. 573-75.

20. N.C. Machingawuta, S. Bagha and P. Grieveson: "Heat Transfer Simulation for Continuous Casting", *Steelmaking Conference Proceedings*, (Washington, D.C., USA), 1991, vol. 74, pp. 163-70.

21. T. Cimarelli: "Mould powder influence on continuous casting operations and on slabs surface quality", *Metallurgia Italiana (Italy),* 1997, vol. 89 (9), pp. 31-37.

22. J. Cho, H. Shibata, T. Emi and M. Suzuki: "Thermal resistance at the interface between mold flux film and mold for continuous casting of steels", *ISIJ International (Japan),* 1998, vol. 38 (5), pp. 440-46.

23. J.F. Chavez, A. Rodriguez, R. Morales and V.H. Tapia: "Laboratory and plant studies on thermal properties of mold powders", *Steelmaking Conference Proceedings*, (Nashville, Tennessee, USA), 1995, vol. 78, pp. 679-86.

24. A. Yamauchi, K. Sorimachi and T. Yamauchi: "Effect of Solidus Temperature and Crystalline Phase of Mould Flux on Heat Transfer in Continuous Casting Mould", *ironmaking and Steelmaking,* 2002, vol. 29 (3), pp. 203-07.

25. D.T. Stone and B.G. Thomas: "Measurement and modeling of heat transfer across interfacial mold flux layers", *Canadian Metallurgical Quarterly (Netherlands),* 1999, vol. 38 (5), pp. 363-75.

26. M. Suzuki, H. Mizukami, T. Kitagawa, K. Kawakami, S. Uchida and Y. Komatsu: "Development of a new mold oscillation mode for high-speed CC of steel slabs", *ISIJ International (Japan),* 1991, vol. 31 (3), pp. 254-61.

27. Y. Nakamori, Y. Fujikake and K. Tokiwa: "Development of Friction Measuring System in a Continuous Casting Mold", *Tetsu-to-Hagane (J. Iron Steel Inst. Jpn.),* 1984, vol. 70 (9), pp. 1262-68.

28. J.A. DiLellio and G.W. Young: "Asymptotic model of the mold region in a continuous steel caster", *Metallurgical and Materials Transactions B: Process Metallurgy and Materials Processing Science,* 1995, vol. 26B (6), pp. 1225-441.

29. M.M. Wolf: "Review of Mould Fricrtion", *BHM,* 2000, vol. 145 (7), pp. 270-75.

30. M.R. Ozgu and B. Kocatulum: "Thermal Analysis of the Burns Harbor No. 2 Slab Caster Mold", *76th Steelmaking Conference*, (Dallas, Texas, USA), 1993, vol. 76, pp. 301-08.

31. G.A. Geist: "Establishing mold thermal stability and lubrication during continuous casting of high carbon steel grades", *83rd Steelmaking Conference*, (Pittsburgh, PA, USA), 2000, vol. 83, pp. 389-96.

32. R.J. O'Malley: "Observations of various steady state and dynamic thermal behaviors in a continuous casting mold", *82nd Steelmaking Conference*, (Chicago, IL, USA), 1999, vol. 82, pp. 13-33.

33. B. Mairy, D. Ramelot and M. Dutrieux: "Mold Lubrication and Oscillation Monitoring for Optimizing Continuous Casting", *5th Process Technology Conference: Measurement and Control Instrumentation in the Iron and Steel Industry*, (Detroit, Michigan, USA), 1985, pp. 101-17.

34. W.H. Emling and S. Dawson: "Mold Instrumentation for Breakout Detection and Control", *74th Steelmaking Conference*, (Washington, D.C., USA), 1991, vol. 74, pp. 197-217.

35. M.S. Bhamra, M.G. Charlesworth, S. Wong, D. Sawyers-Villers and A.W. Cramb: "Crystallization of fluxes under varying cooling rates", *54th Electric Furnace Conference*, (Dallas, Texas, USA), 1996, vol. 54, pp. 551-64.

36. C. Orrling, A.W. Cramb, A. Tilliander and Y. Kashiwaya: "Observations of the melting and solidification behavior of mold slags", *Iron and Steelmaker (USA),* 2000, vol. 27 (1), pp. 53-63.

37. Y. Meng and B.G. Thomas: "Heat Transfer and Solidification Model of Continuous Slab Casting: CON1D", *Metall. Mater. Trans. B (USA),* 2003, (accepted).

38. S. Itoyama, M. Washio and H. Nishikawa: "Reduction of Friction Force in Mold and Prevention of Sticking Type Breakout for High Speed CC of Slabs", *Tetsu-to-Hagane (J. Iron Steel Inst. Jpn.),* 1988, vol. 74 (7), pp. 1274-81.

39. L. Hering and H.W. Fenzke: "On-Line Monitoring of Heat Flow Density in Slab Continuous Casting", *Stahl und Eisen (Germany),* 1992, vol. 112 (7), pp. 91-95.

40. G.J.W. Kor: "An Analysis of the Fluid Flow of Liquid Mold Powder in the Space Between the CC Mold and the Steel Shell", *Continuous Casting of Steel, 2nd Process Technology Conf.*, (Chicago, Ill., USA), 1981, vol. 2, pp. 124-32.

41. D.R. Bland: "Flux and the Continuous Casting of Steel", *IMA Journal of Applied Mathematics,* 1984, vol. 32, pp. 89-112.

42. H. Nakato, T. Nozaki, Y. Habu and H. Oka: "Improvement of Surface Quality of Continuously Cast Slabs by High Frequency Mold Oscillation", *68th Steelmaking Conference*, (Detroit, Michigan, USA), 1985, vol. 68, pp. 361-65.

43. E. Anzai, T. Shigezumi, T. Nakano, T. Ando and M. Ikeda: "Hydrodynamic Behavior of Molten Powder in Meniscus Zone of Continuous Casting Mold", *Nippon Steel Tech. Rep.,* 1987, (34), pp. 31-40.

44. R. Bommaraju and E. Saad: "Mathematical Modelling of Lubrication Capacity of Mold Fluxes", *73th Steelmaking Conference*, (Detroit, Michigan, USA), 1990, vol. 73, pp. 281-96.

45. I.B. Risteski: "A Mathematical Model of the Movement of Molten Powder in the Vicinity of the Meniscus During the Continuous Casting of Steel", *Revista de Metalurgia (Spain),* 1992, vol. 28 (5), pp. 288-96.

46. J.M. Hill and Y.H. Wu: "On a Nonlinear Stefan Problem Arising in the Continuous Casting of Steel", *Acta mech.,* 1994, vol. 107 (1-4), pp. 183-98.

47. J.F. Chavez, A. Celaya, M.A. Barron and R.D. Morales: "Heat transfer in mold flux-layers during slab continuous casting", *Seventy Ninth Conference of the Steelmaking Division of the Iron and Steel Society*, (Pittsburgh, Pennsylvania, USA), 1996, vol. 79, pp. 321-29.

48. K. Takashi, H. Sei, K. Masayuki, N. Ken, H. Kazuharu and M. Toshihiko: "Behavior of lubrication and heat transfer in mold at high speed continuous casting", *Tetsu-to-Hagane (Journal of the Iron and Steel Institute of Japan) (Japan),* 1997, vol. 83 (11), pp. 701-06.

49. S. Ogibayashi: "Mathematical Modeling of Mold Powder Infiltration and Heat Extraction Near Meniscus in Continuous Casting", *85th Steelmaking Conference*, (Nashville, TN, USA), 2002, vol. 85, pp. 175-83.

50. K. Nakajima: "Heat transfer and lubrication behavior in mold at high-speed continuous casting of steel slabs", *Curr. Adv. Mater. Process.,* 1992, vol. 5 (4), pp. 1221-24.

51. P.V. Riboud, Y. Roux, L.D. Lucas and H. Gaye: "Improvement of Continuous Casting Powders", *Fachberichte Huttenpraxis Metallweiterverarbeitung,* 1981, vol. 19 (8), pp. 859-69.

52. M.D. Lanyi and C.J. Rosa: "Viscosity of Casting Fluxes Used During Continuous Casting of Steel", *Metall. Trans. B,* 1981, vol. 12B (2), pp. 287-98.

53. W.L. McCauley and D. Apelian: "Temperature Dependence of the Viscosity of Liquids", *Proceeding of 2nd International Symposium on Metallurgical Slags and Fluxes*, 1984, pp. 925-47.

54. K.C. Mills and S. Sridhar: "Viscosities of ironmaking and steelmaking slags", *Ironmaking and Steelmaking (UK),* 1999, vol. 26 (4), pp. 262-68.

55. *MATLAB6.1 Users Manual*, The Mathworks, INC, 2001.

56. *ANSYS6.1 Users Manual*, ANSYS, Inc, 2002.

57. K. Schwerdtfeger and H. Sha: "Depth of oscillation marks forming in continuous casting of steel", *Metallurgical and Materials Transactions B (USA),* 2000, vol. 31B (4), pp. 813-26B.

58. J. Watzinger and A. Flick: "Online mold friction monitoring system in continuous casting", *84th Steelmaking Conference*, (Baltimore, MD, USA), 2001, vol. 84, pp. 205-13.

59. D. Larson: "Criteria for Selecting Mold Powders to Optimize Continuous Cast Steel Quality", *Industrial Heating,* 1986, vol. 53 (4), pp. 16-17.

60. K.J. Lin and Y.H. Chung: "Selection of Casting Powder", *China Steel Technical Report (Republic of China),* 1992, (6), pp. 71-79.

61. F. Shahbazian, D. Sichen and S. Seetharaman: "The effect of addition of Al2O3 on the viscosity of CaO-'FeO'-SiO2 -CaF2 slags", *ISIJ Int. (Japan),* 2002, vol. 42 (2), pp. 155-62.

62. Q. Wang, B. Xie and J. Chi: "Study on CC fluxes with high basic and high glassy properties", *Conference on Continuous Casting of Steel in Developing Countries*, (Beijing, China), 1993, pp. 842-51.

63. Y. Kashiwaya, C.E. Cicutti and A.W. Cramb: "An investigation of the crystallization of a continuous casting mold slag using the single hot thermocouple technique", *ISIJ International (Japan),* 1998, vol. 38 (4), pp. 357-65.

64. C. Orrling, S. Sridhar and A.W. Cramb: "In situ observation of the role of alumina particles on the crystallization behavior of slags", *ISIJ International (Japan),* 2000, vol. 40 (9), pp. 877-85.

65. M.S. Jenkins and B.G. Thomas: "An Investigation of Some Mold Powder Related Startup Problems", *Steelmaking Conference Proceeding 1997*, (Chicago, IL, USA), 1997, vol. 80, pp. 285-93.

66. S. Ogibayashi, T. Mukai and Y. Mimura: "Mold Powder Technology for Continuous Casting of Low-Carbon Aluminium-Killed Steel", *Nippon Steel Tech. Rep.,* 1987, (34), pp. 1-10.

67. K. Tsutsumi, H. Murakami, S.I. Nishioka, M. Tada, M. Nakada and M. Komatsu: "Estimation of mold powder consumption in continuous casting", *Tetsu-to-Hagane (Journal of the Iron and Steel Institute of Japan) (Japan),* 1998, vol. 84 (9), pp. 617-24.

68. C.A. Pinheiro, I.V. Samarasekera and J.K. Brimacombe: "Mold flux for continuous casting of steel", *Iron and Steelmaker (USA),* 1995, vol. 22 (12), pp. 43-44.

69. H. Abratis, F. Hofer, M. Junemann, J. Sardemann and H. Stoffel: "Heat transfer at the continuous casting permanent mold for different slag producing powder additives", *Stahl und Eisen (Germany),* 1996, vol. 116 (9), pp. 73-78.

70. A. Yamauchi: *Heat transfer phenomena and mold flux lubrication in continuous casting of steel*, PhD Thesis, Royal Institute of Technology, 2001.

71. H. Nakato, S. Omiya, Y. Habu, K. Hamagami and T. Koshikawa: "Optimizing Mold Lubrication for High-Speed Continuous Casting of Slabs", *Journal of metals,* 1984, vol. 36 (3), pp. 44-50.

72. K. Hamagami, K. Sorimachi, M. Kuga, T. Koshikawa and M. Saigusa: "Studies on Quality Improvement in Strand cast Slabs at Chiba Works", *Steelmaking Conference*, 1982, vol. 65, pp. 358-64.

73. T. Okazaki, H. Tomono, K. Ozaki and H. Akahane: "Effect of Short Stroke High Cycle Oscillation on the Strand Surface Quality", *Tetsu-to-Hagane (J. Iron Steel Inst. Jpn.),* 1982, vol. 68 (10), p. 265.

74. M. Inagaki: "Improvement Technology of Surface Quality at Velocity Change", *CAMP-ISIJ,* 1989, (2), p. 309.

75. B. Ho: *Characterization of Interfacial Heat Transfer in the Continuous Slab Casting Process*, Master Thesis, UIUC, 1992.

76. D.P. Lorento: *Internal Report*. 2001.

77. C. Li and B.G. Thomas: "Analysis of the potential productivity of continuous cast molds", *The Brimacombe Memorial Symposium*, (Vancouver, British Columbia, Canada), 2000, pp. 595-611.

78. J.E. Lait, J.K. Brimacombe and F. Weinberg: "Mathematical Modelling of Heat Flow in the Continuous Casting of Steel", *ironmaking and Steelmaking,* 1974, vol. 1 (2), pp. 90-97.

79. M.M. Wolf: "Mold length in slab casting--a review", *Iron and Steelmaker (USA),* 1996, vol. 23, pp. 47-51.

List of Tables and Figures

Table I. Casting Condition and Simulation Parameters

(Case I with Slag A at 1.0m/min)

Carbon Content	$C\%$	0.05	%
Liquidus Temperature	T_{liq}	1529	^{o}C
Solidus Temperature	T_{sol}	1509	^{o}C
Steel Density	ρ_{steel}	7400	kg/m^2
Fraction Solid for Shell Thickness Location	f_s	0.3	-
Mold Powder Solidification Temperature	T_{fsol}	950	^{o}C
Mold Powder Viscosity at 1300^{o}C	μ_{1300}	4.3	Poise
Exponent for Temperature dependence of Viscosity	n	1.6	-
Slag Density	ρ_{slag}	2500	kg/m^3
Mold Powder Conductivity	k_{solid}, k_{liquid}	1.5, 1.5	W/mK
Poisson's Ratio of Slag	υ	0.17	-
Mold Slag Consumption Rate	Q_{slag}	0.41	kg/m^2
Mold Slag Lubrication Consumption Rate	Q_{lub}	0.2	kg/m^2
Solid layer/mold Interface Friction Coefficient	ϕ_{static}, ϕ_{moving}	0.4, 0.4	-
Solid slag layer velocity	V_s	0.	m/s
Casting Speed	V_c	1.0	m/min
Pour Temperature	T_{pour}	1550	^{o}C
Slab Geometry	$W \times N$	1500×230	mm $\times$ mm
Working Mold Length	Z_{mold}	800	mm
Oscillation Mark Geometry	$d_{mark} \times w_{mark}$	0.45×4.5	mm $\times$ mm
Mold Oscillation Frequency	f	83.3	cpm
Oscillation Stroke	s	7.8	mm
Negative Strip Ratio of velocity	$NS\%$	0.3	-
Liquid Slag Pool depth	h_0	10	mm
Time Step	dt	0.002	s
Mesh Size	dx	0.5	mm

Table II. Simulation Parameters in Liquid Slag Layer Model Validation Cases

	Case (a)	Case(b)	Case (c)	Case (d)	
Temperature dependent viscosity exponent, n:	0	1.6	0	1.6	-
Liquid film thickness, dl:	0.2		2.0		mm
Viscosity at shell surface side, μ_s:	0.53		0.50		Pas
Density, ρ_{slag}:	2500		4000		kg/m^3
Casting speed, V_c:	1.0		1.5		m/min
Mold oscillation stroke, s:	7.8		20		mm
Mold oscillation frequency, f:	1.389		1.5		cps
Steel density, ρ_{steel}:	7400		7400		kg/m^3
Time Step, Δt:	5.0E-7				s
Mesh Size, Δx:	0.04				mm

Table III. Terms in Eq.(3) for Case (b) at t=0.18s, x=0.16mm (unit: N/m^3)

$\rho_{slag} \cdot V_z \cdot \frac{\partial V_z}{\partial z}$	$\rho_{slag} \cdot V_y \cdot \frac{\partial V_z}{\partial y}$	$\rho_{slag} \cdot V_z \cdot \frac{\partial V_z}{\partial z}$	$\left(\rho_{slag} - \rho_{steel}\right) \cdot g$	$\frac{\partial \tau_{yz}}{\partial y}$	$\frac{\partial \tau_{zz}}{\partial z}$
-335.	0.0304	0.0431	-48020.	47683.	-1.0624

Table IV. Slag Composition and Properties

Slag	CaO	SiO_2	Al_2O_3	MgO	Na_2O	K_2O	F_2	FeO	MnO	B_2O_3	T_{fsol}	n	μ_{1300}
	wt%	wt%	wt%	wt%	wt%	wt%	wt%	wt%	wt%	wt%	°C	-	P
A	32.3	36.4	8.9	0.7	5.0	1.9	8.3	3.0	-	3.4	950	1.6	4.3
G	27.5	30.3	21.4	0.9	5.6	-	12.0	1.1	1.3	-	850	3.2	5.0
C	34.8	38.3	0. 5	1.2	7.1	-	15.2	1.4	1.6	-	980	1.6	1.7

Table V. Case Study Parameters

	Case I	Case II	Case III
Lubrication Consumption, Q_{lub}:	0.2kg/m^2	critical	0.2kg/m^2
Solid Layer Status:	attached	attached	moving

Table VI. Mold Oscillation Practice with Casting Speed

Casting Speed, V_c	Oscillation frequency, f	Negative Strip Time, NST	Negative Strip ratio, $NS\%$	Osc. Mark, $d_{mark} \times w_{mark}$	Osc. Marks Consumption, Q_{oscg}
m/min	cpm	s	-	mm × mm	kg/m^2
1.0	83.3	0.24	0.3	.45*4.5	0.21
1.3	108.3	0.19	0.3	.30*3.0	0.094
1.6	133.3	0.15	0.3	.16*1.6	0.027
2.0	166.7	0.12	0.3	0*0	0
3.0	250.0	0.08	0.3	0*0	0
5.0	416.7	0.05	0.3	0*0	0

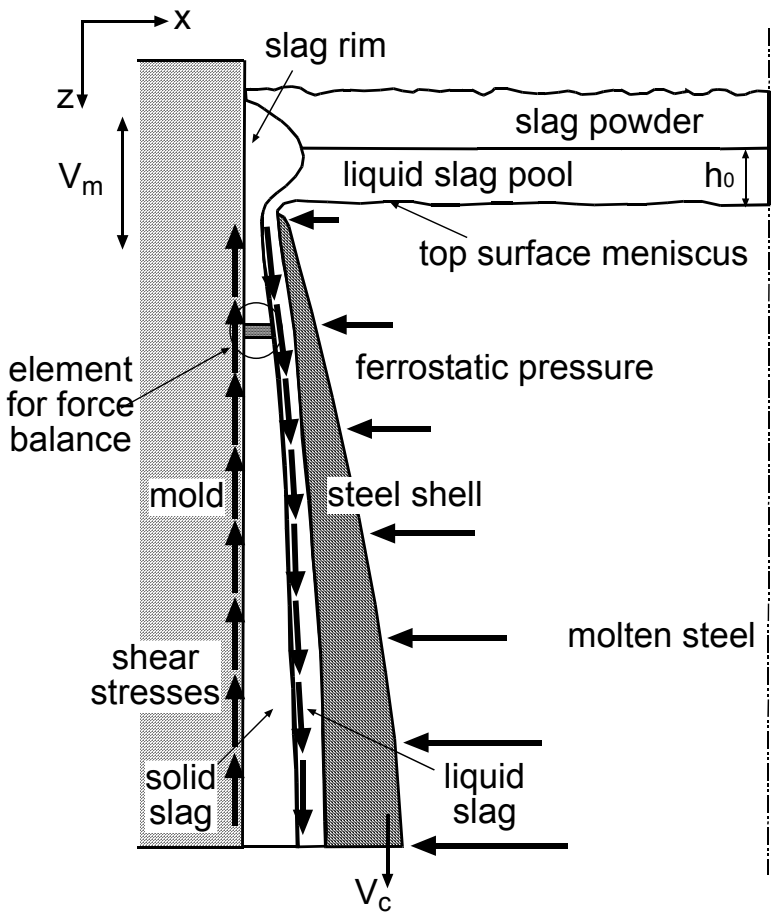

Fig. 1-Schematic of interfacial gap phenomena in continuous casting mold

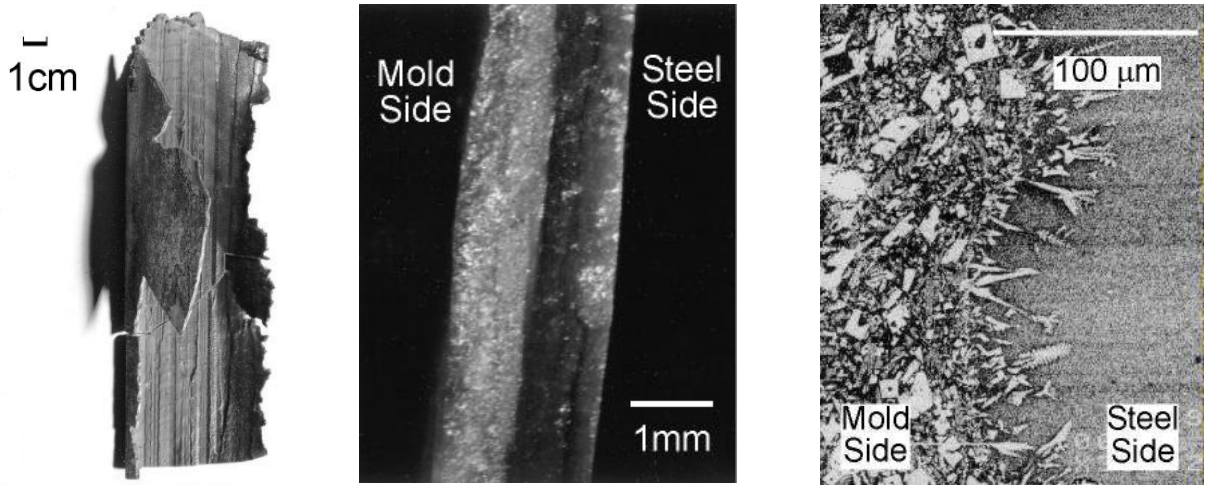

(a) macroscopic film including corner

(b) crystalline and glassy layers

(c) close-up of the crystalline layer growing into glassy layer

Fig. 2-Sample of slag layer and microstructure

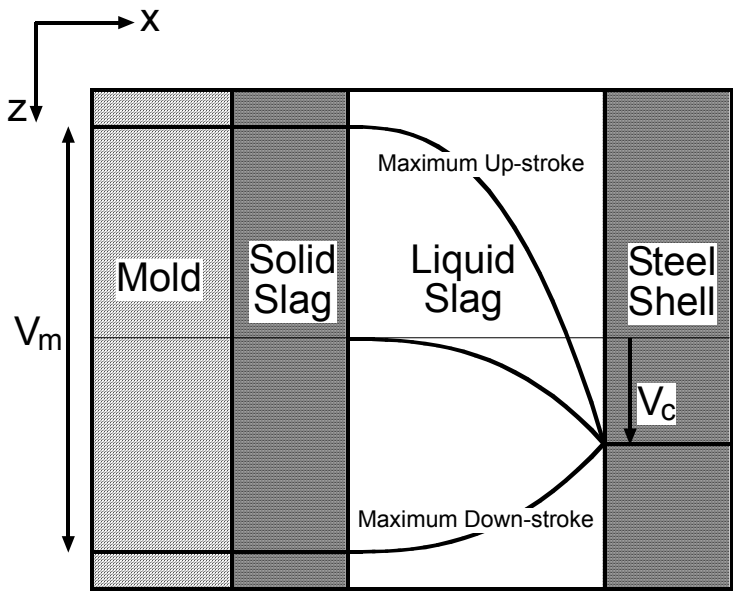

Fig. 3-Schematic profile of slag velocity during oscillation cycle

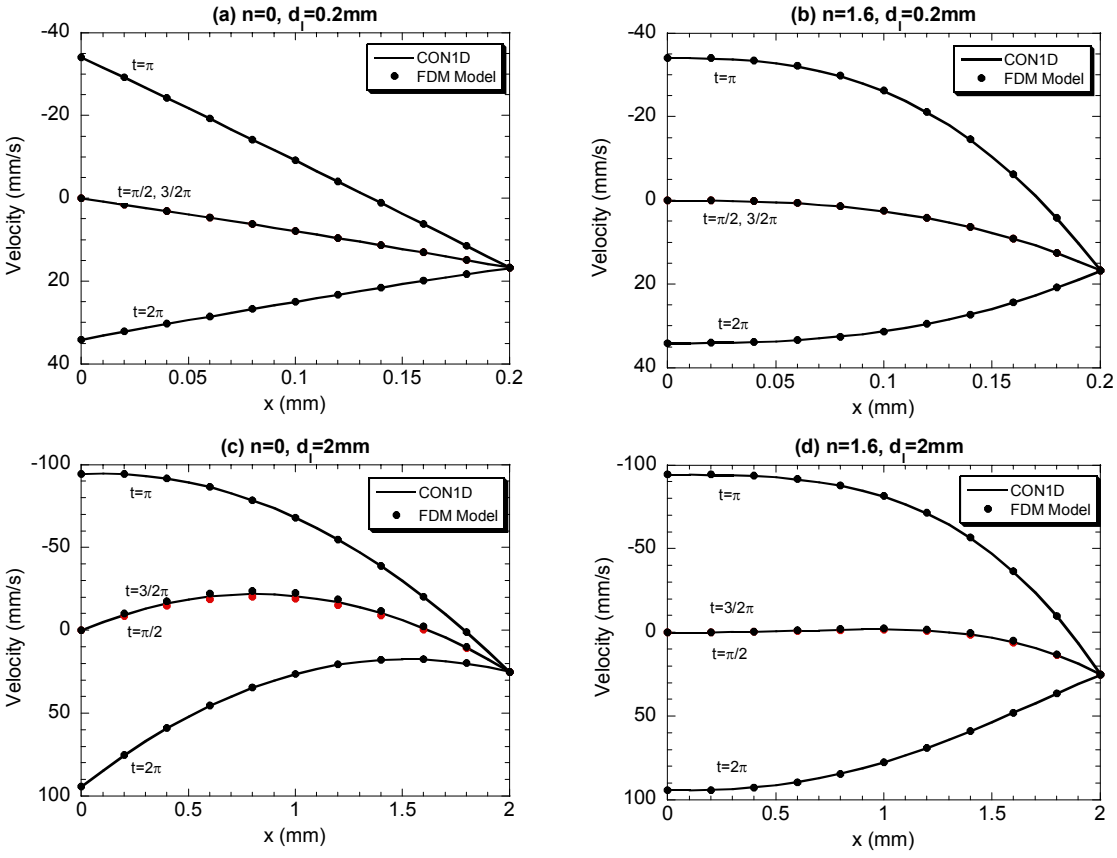

Fig. 4-Velocity profiles in liquid flux layer
(for different viscosity exponent(0/1.6) and film thickness (0.2/2mm))

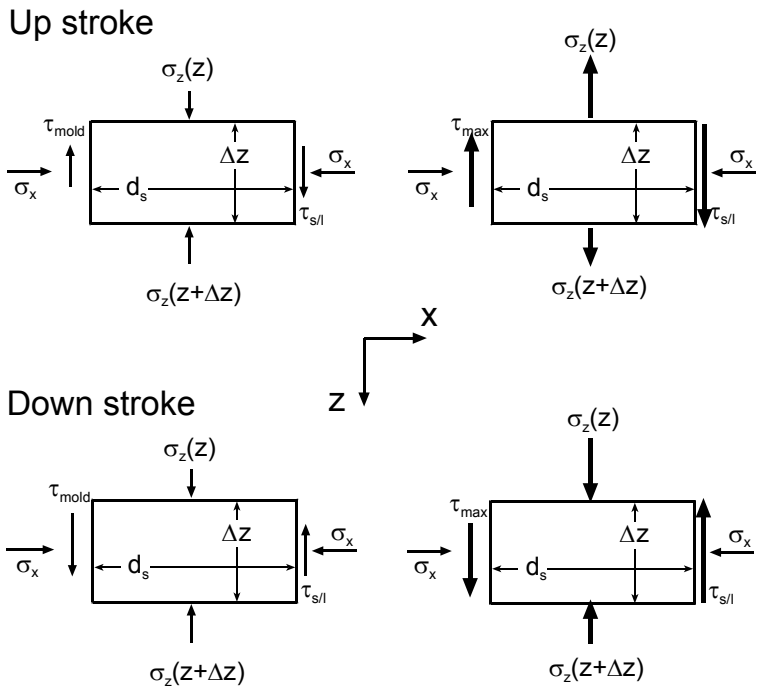

(a) liquid shear stress limited (b) friction coefficient limited

Fig. 5-Force balance on solid slag layer section (mold wall friction left, liquid layer shear stress right and axial stress)

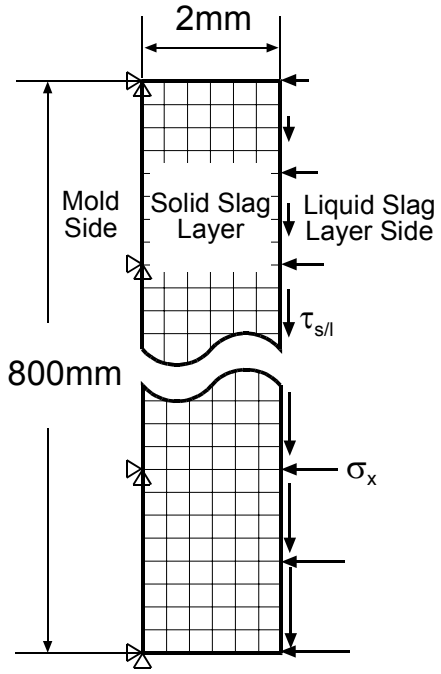

Fig. 6-ANSYS solid slag stress model domain, mesh and BCs

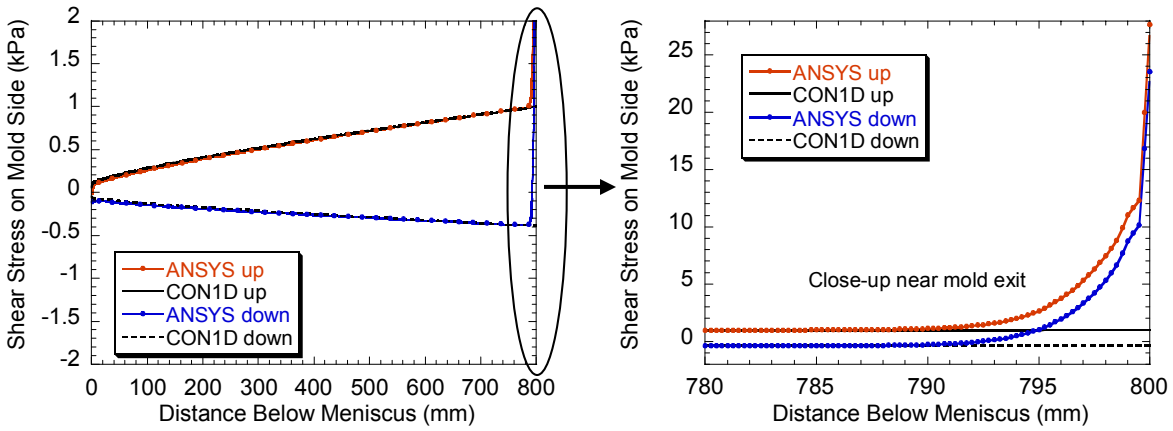

(a) Shear stress on mold side

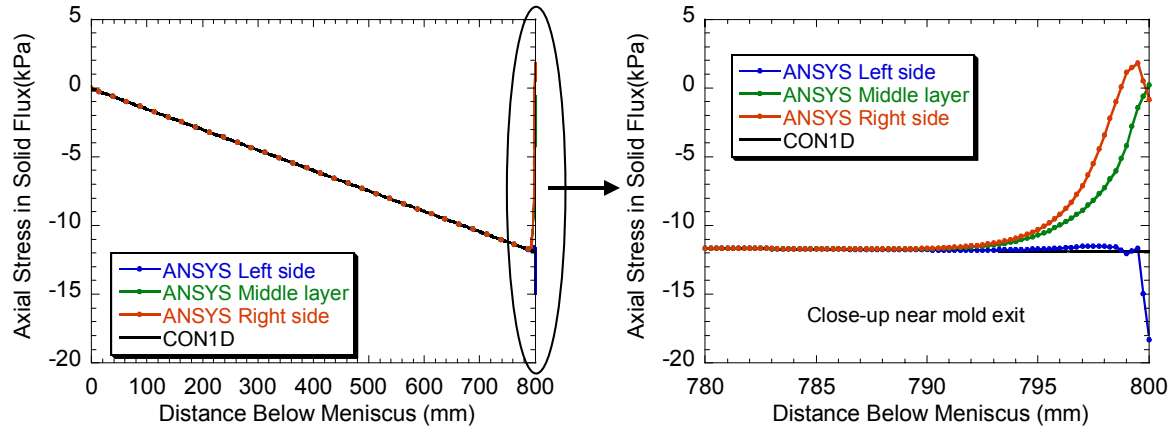

(b) Axial stress in solid slag

Fig. 7-Comparison of CON1D & ANSYS results (Case I with Slag A)

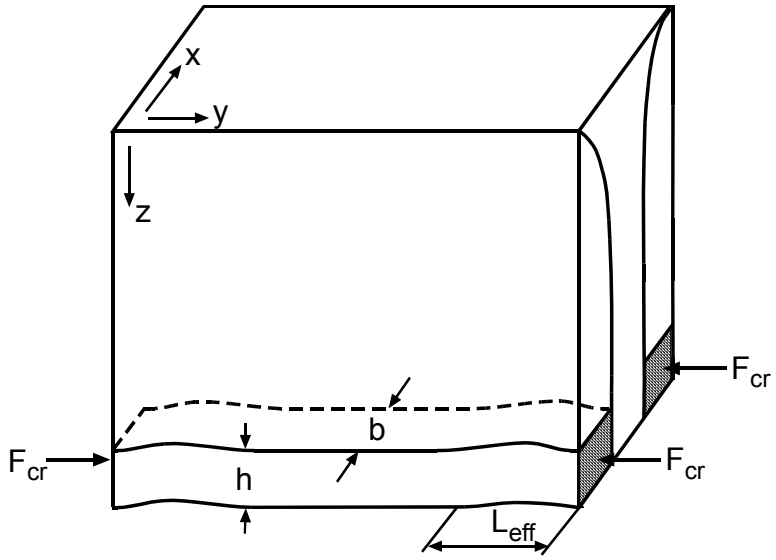

Fig. 8-Schematic of friction forces from excessive taper of narrow mold faces

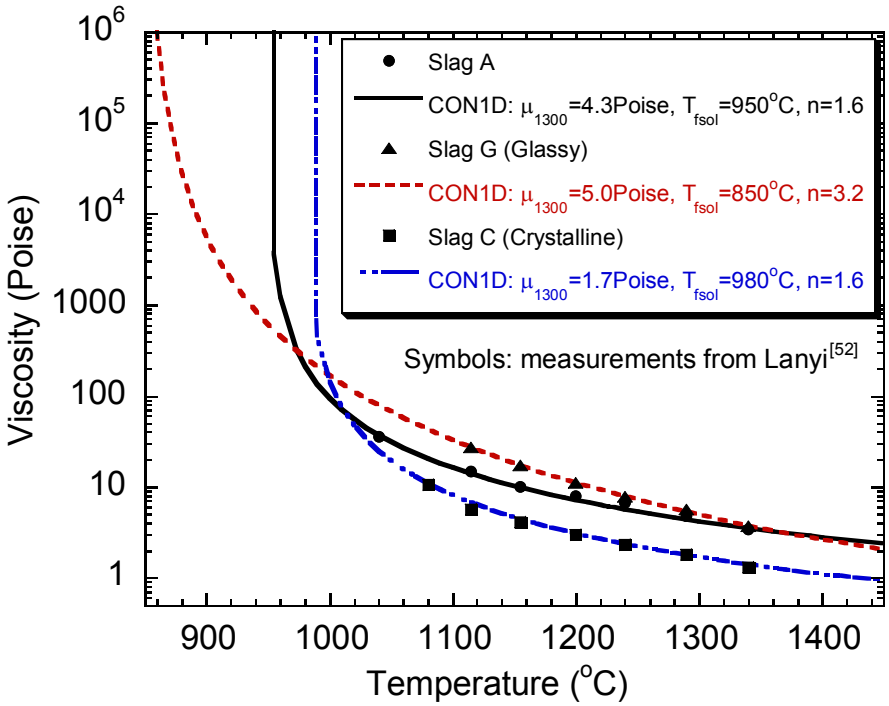

Fig. 9-Mold slag viscosities modeled in this work

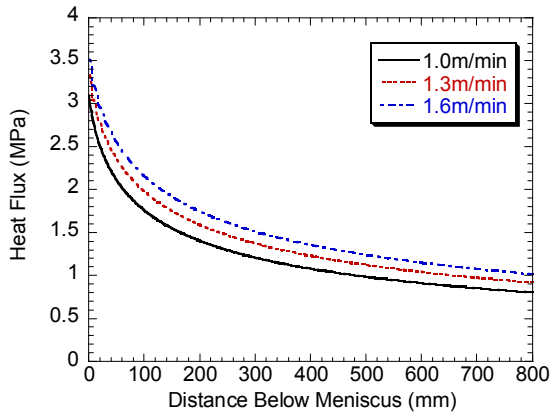

(a) Heat Flux

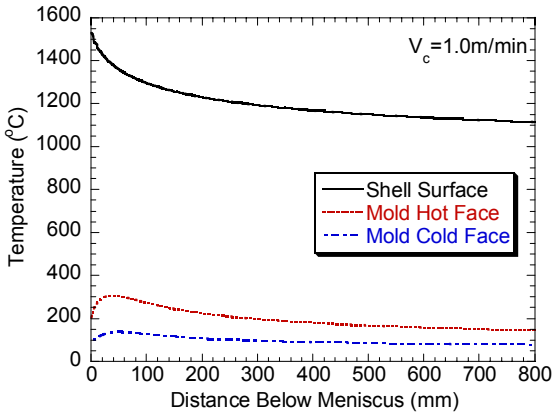

(b) Shell and Mold Temperature

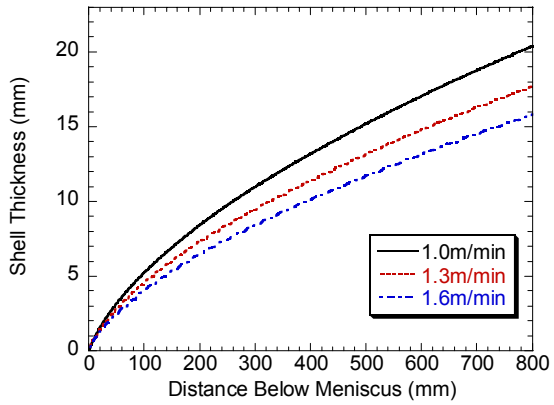

(c) Steel Shell Thickness

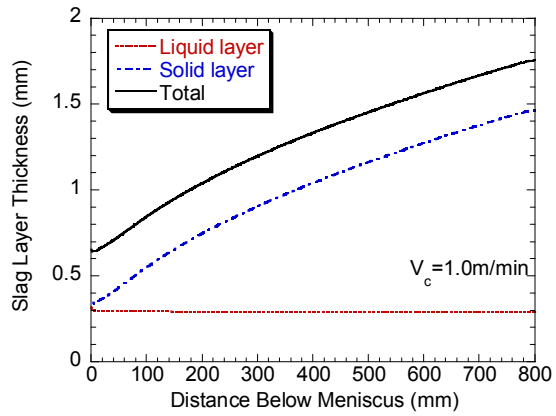

(d) Slag Layer Thickness

Fig. 10-Typical results of Case I with Slag A

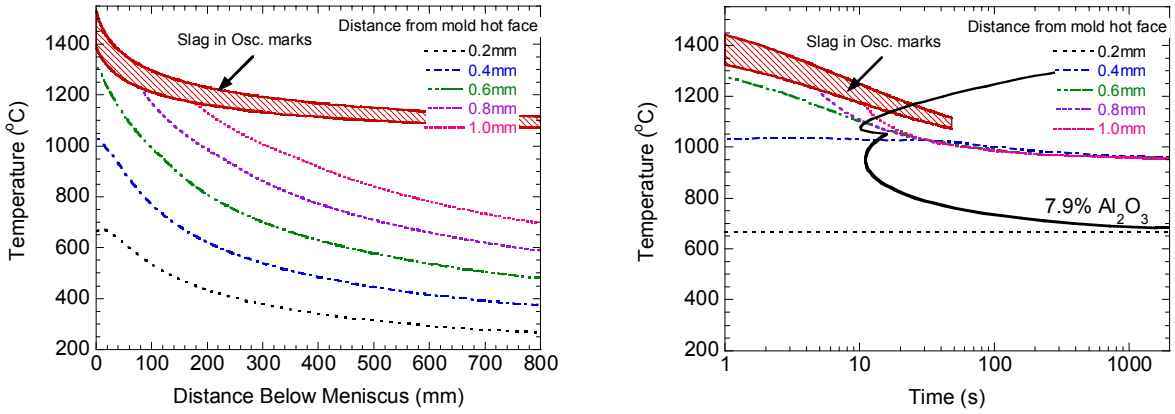

(a) Slag A (Crystalline)

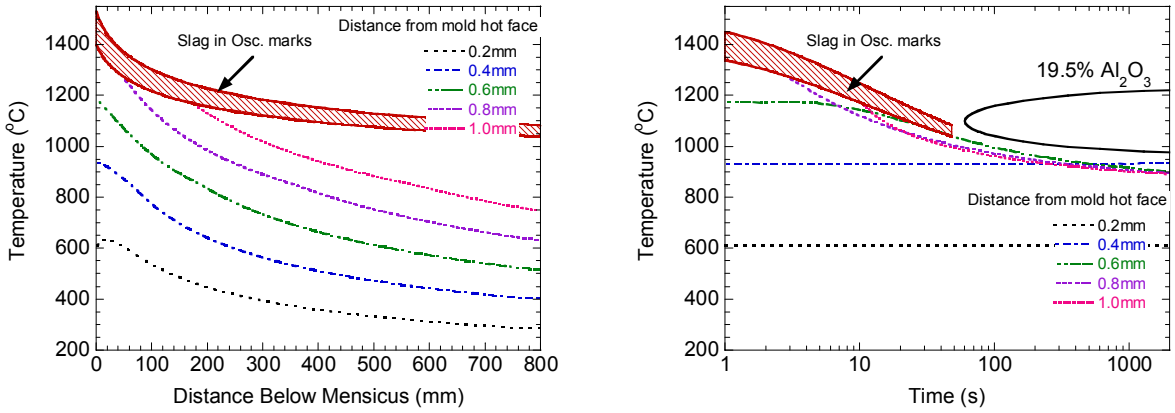

(b) Slag G (Glassy)

Fig. 11-Slag layer cooling history with attached slag (Case I) and measured TTT curves

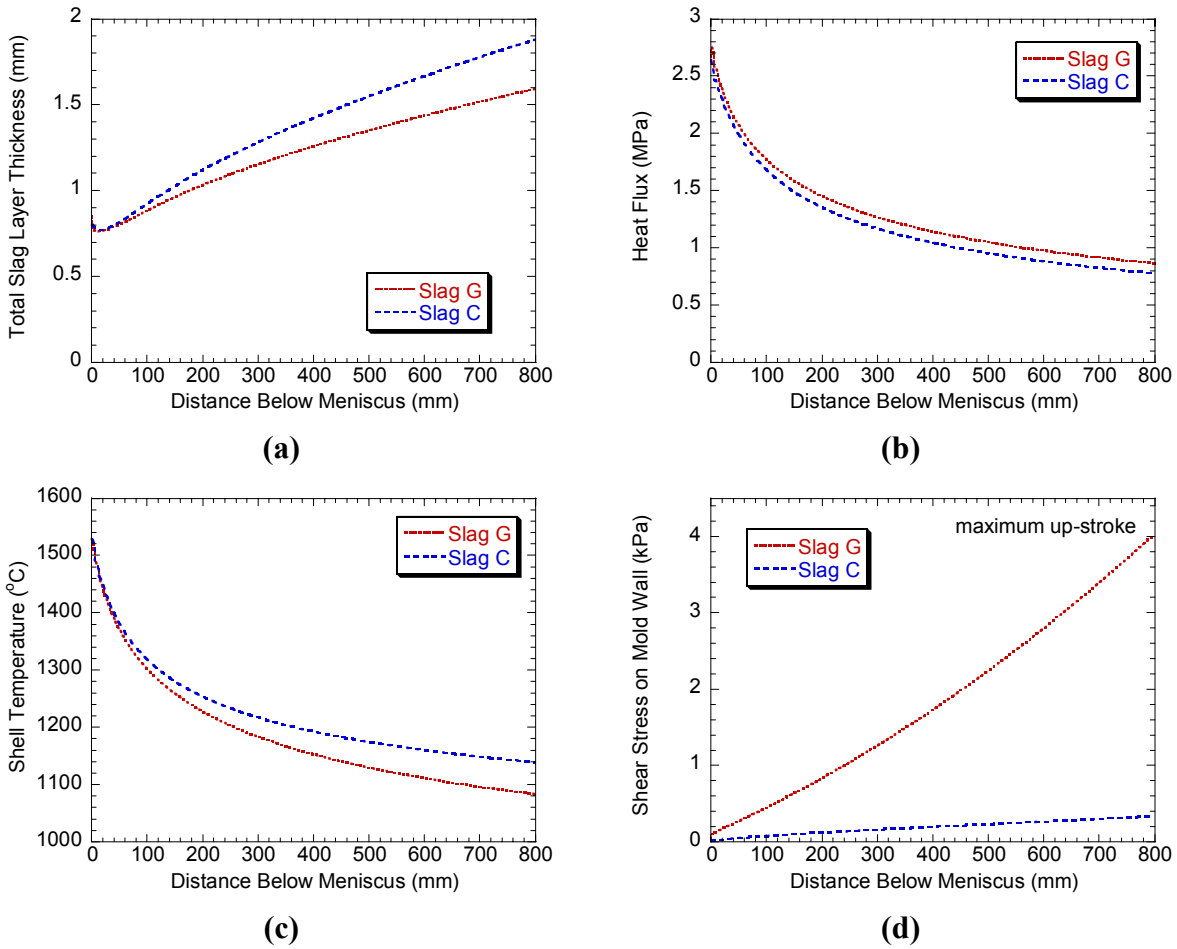

Fig. 12-Effects of slag type on slag layer thickness, friction, heat flux and shell temperature

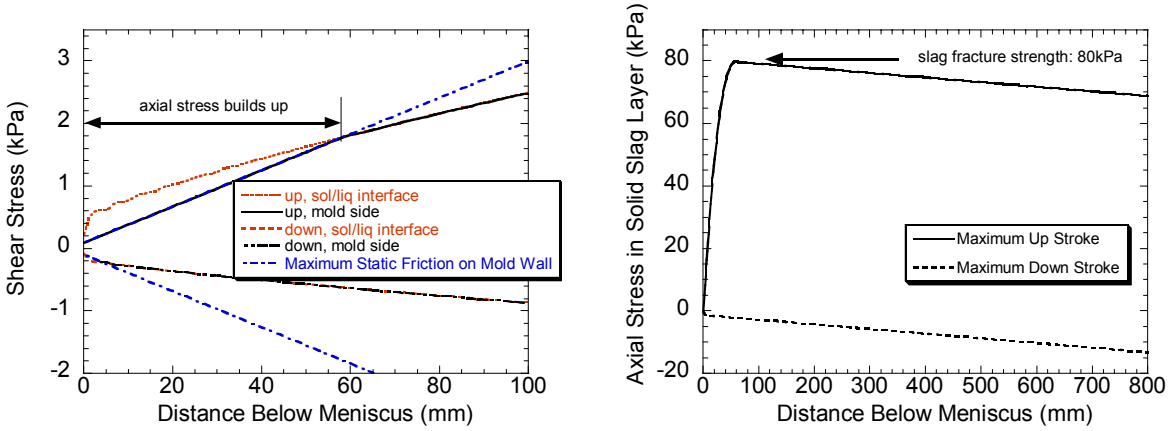

(a) Slag A

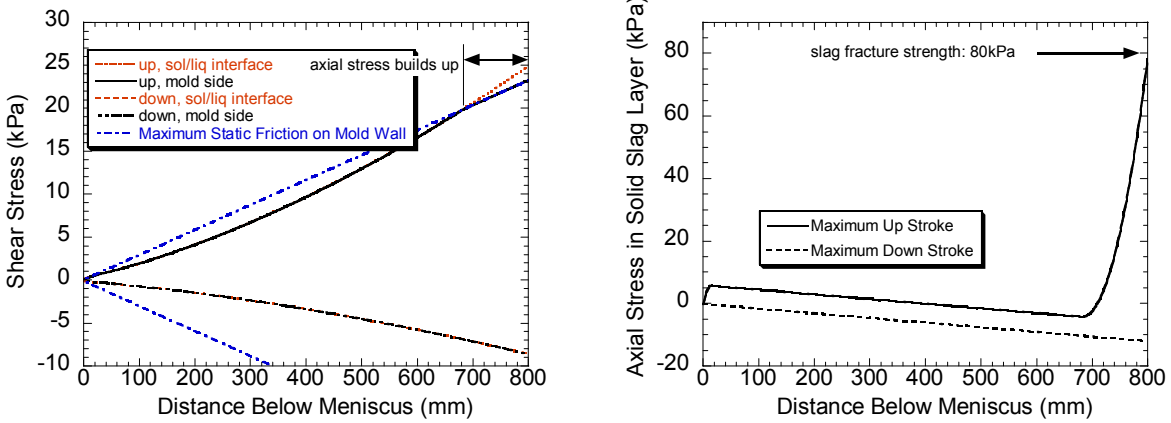

(b) Slag G

Fig. 13-Effect of Slag type on axial stress build up in solid layer for critical Q_{lub}(Case II)

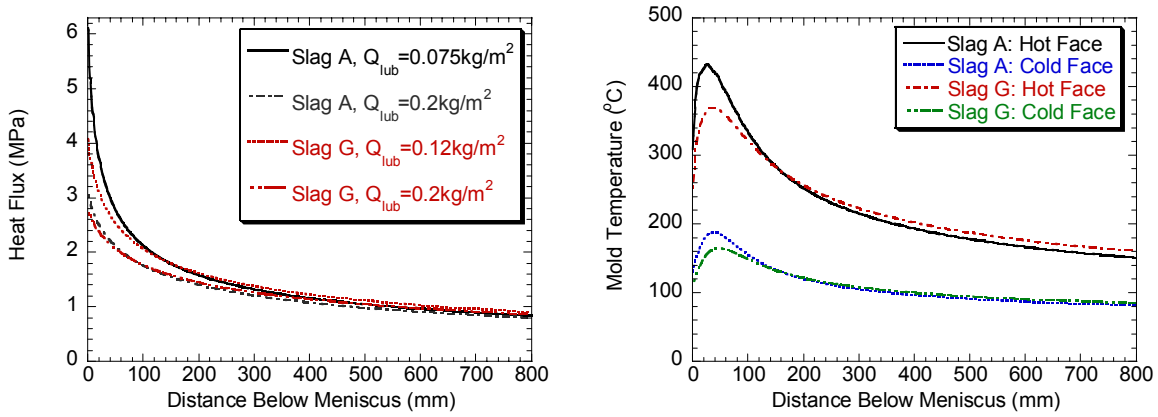

(a) Heat flux **(b) Mold temperature**

Fig. 14-Comparison of heat flux and mold temperature with critical consumption rate (Case II)

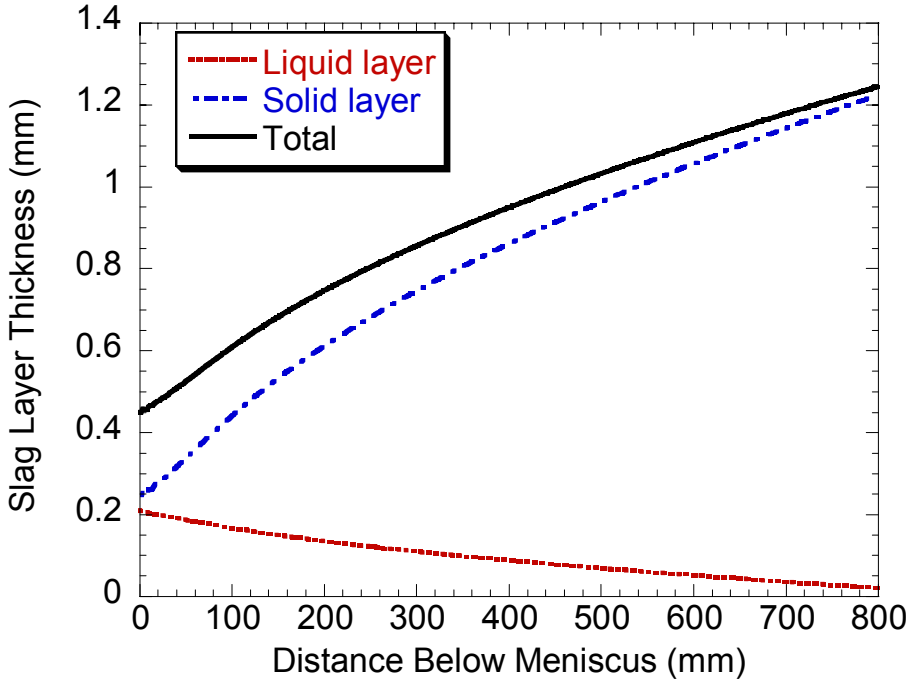

Fig. 15-Slag layer thickness with "moving" solid layer (Case III with Slag A)

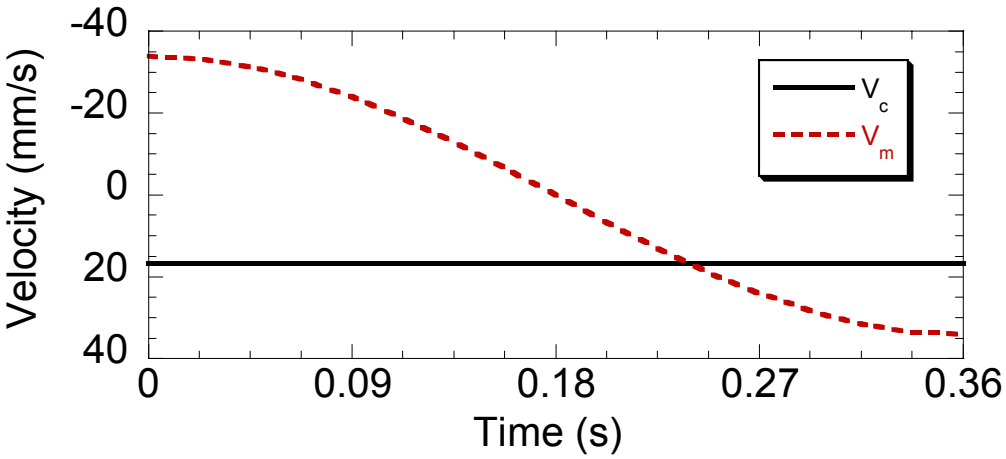

(a) Casting speed and mold velocity

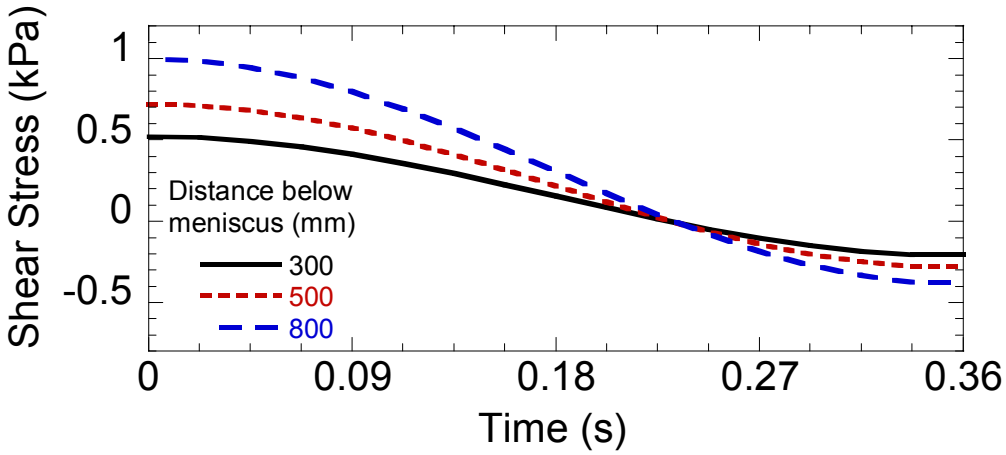

(b) Attached solid layer (Case I)

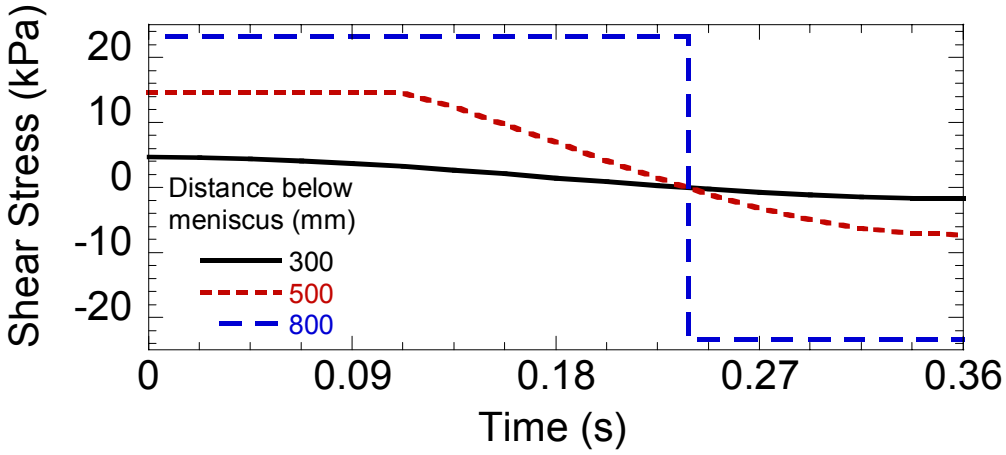

(c) "Moving" solid layer (Case III)

Fig. 16-Velocity and shear stress during half oscillation cycle (Slag A)

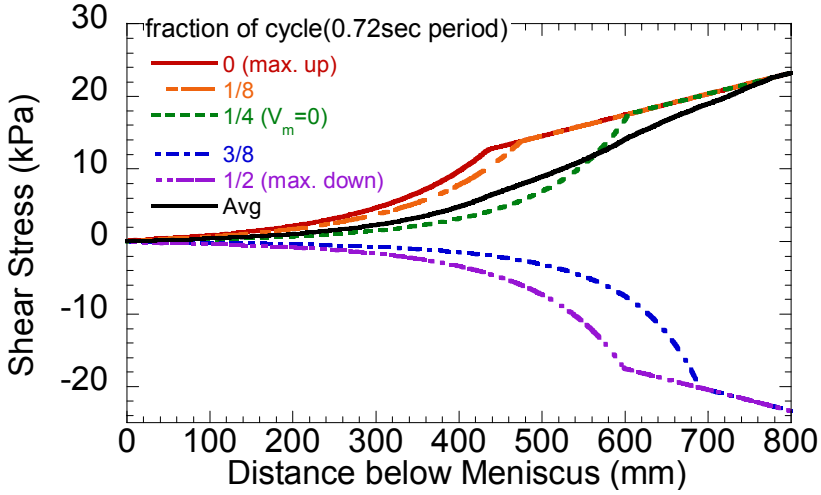

Fig. 17-Shear stress down the mold wall with "moving" solid layer (Slag A)

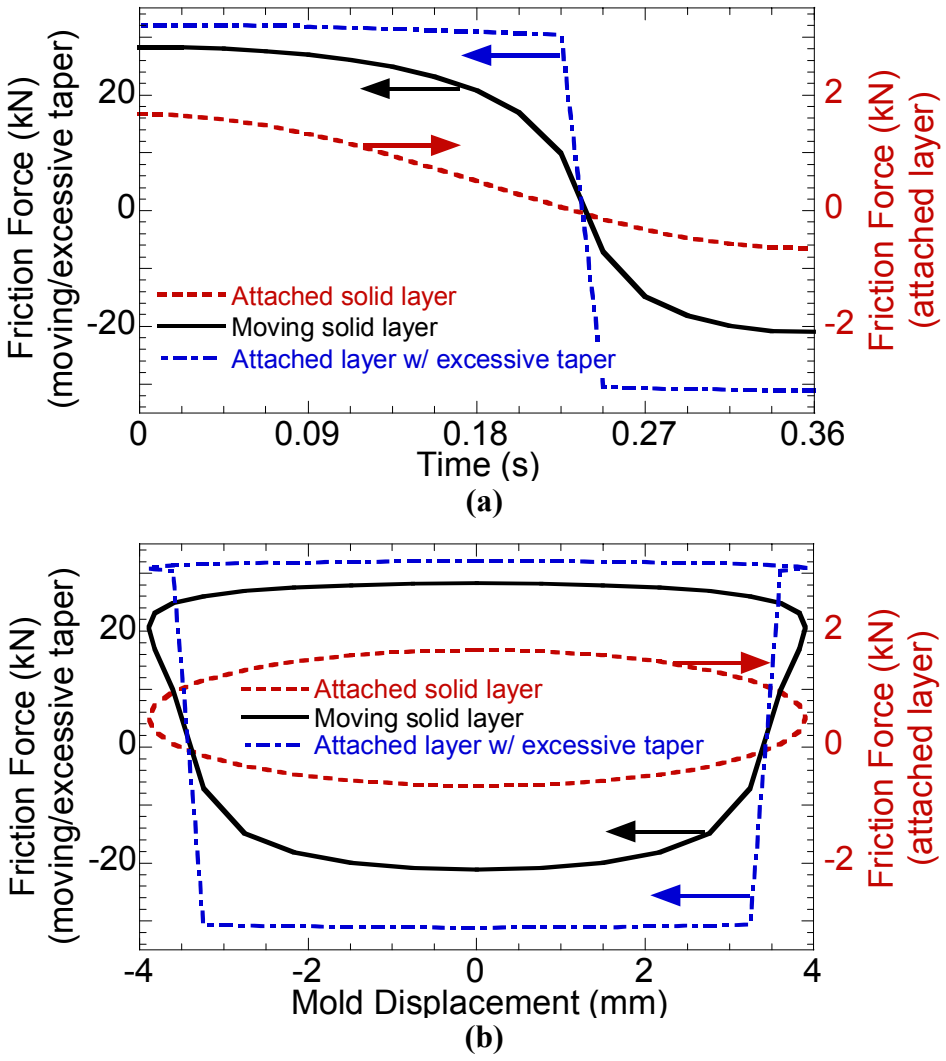

Fig. 18-Friction force over oscillation cycle (Slag A)

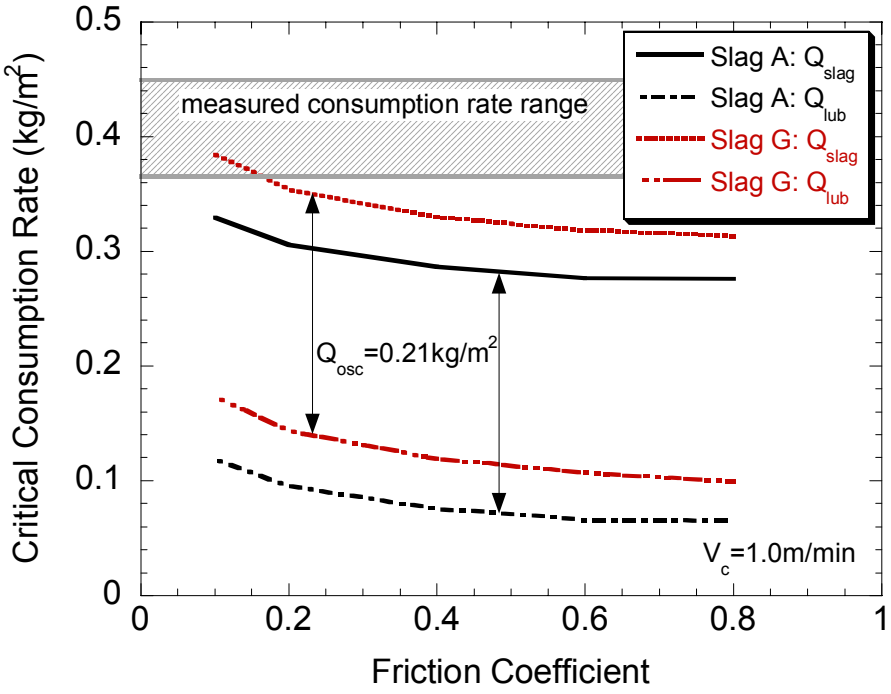

Fig. 19-Effect of friction coefficient on critical consumption rate

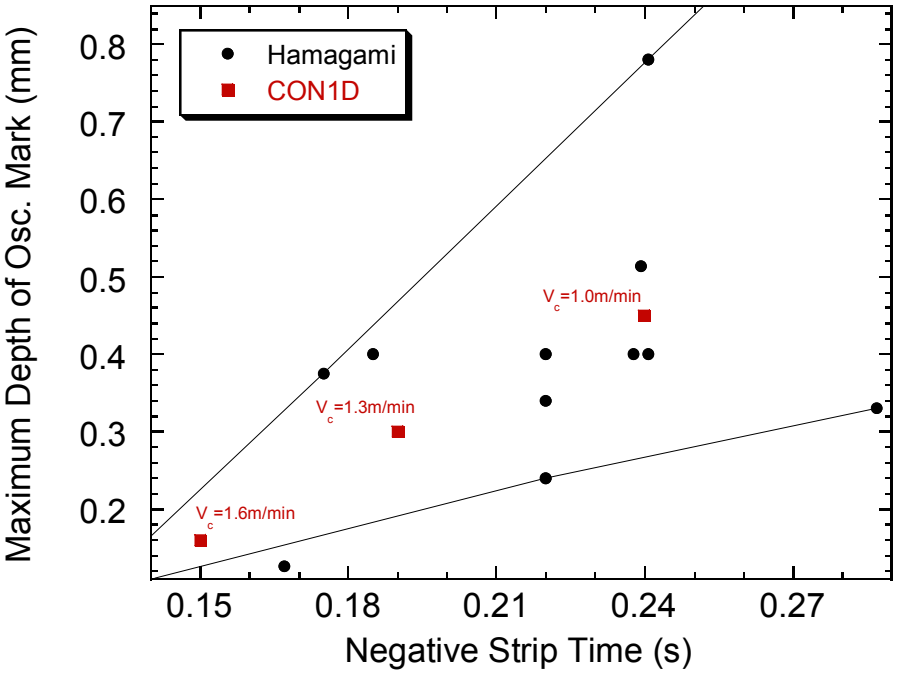

Fig. 20-Maximum oscillation mark depth

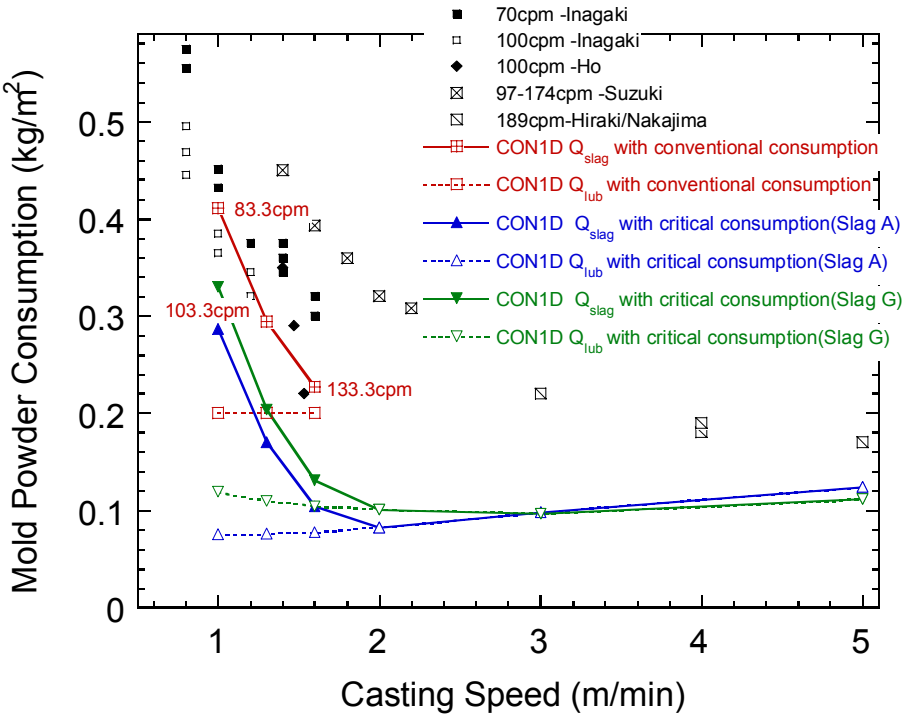

Fig. 21-Powder consumption rates

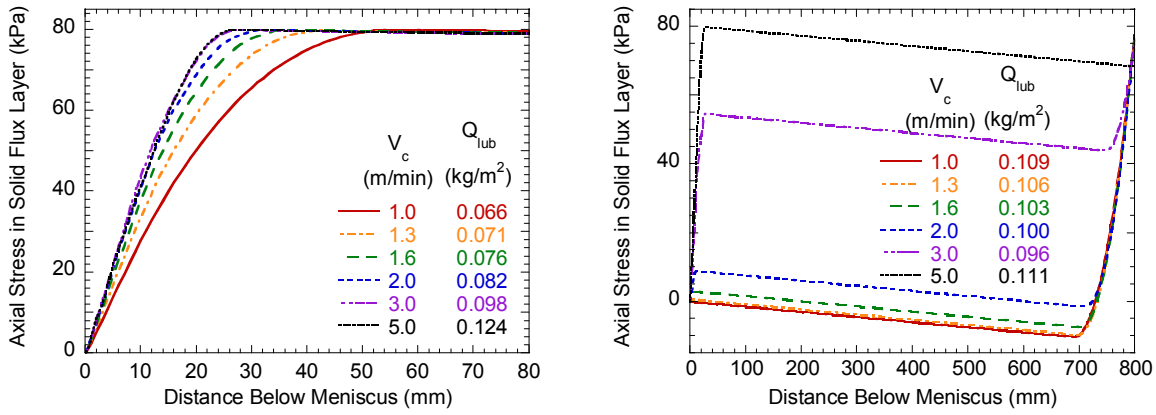

(a) Slag A **(b) Slag G**

Fig. 22-Effect of casting speed on solid slag fracture (no oscillation marks)

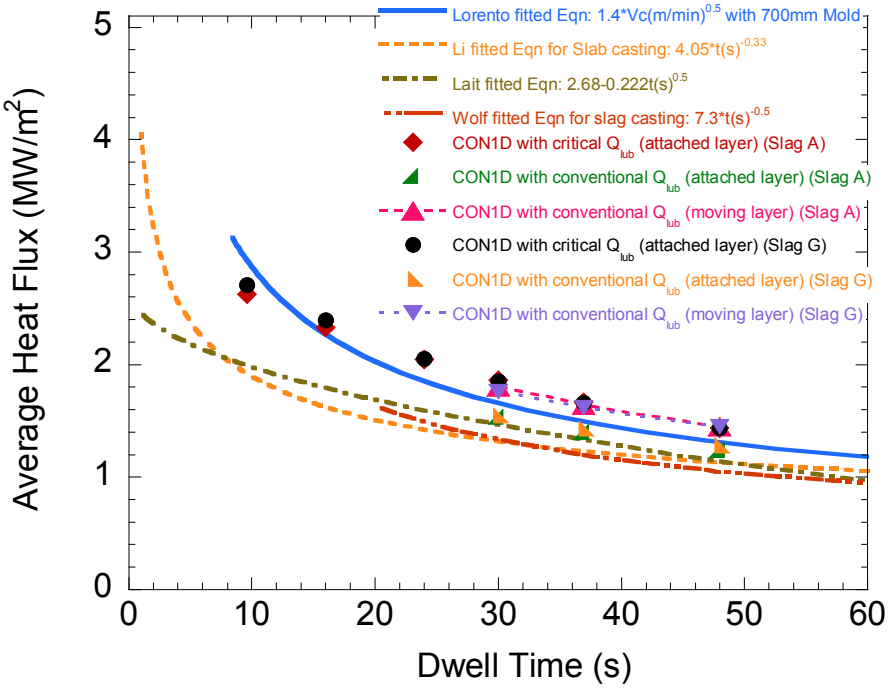

Fig. 23-Average heat flux vs. casting speed

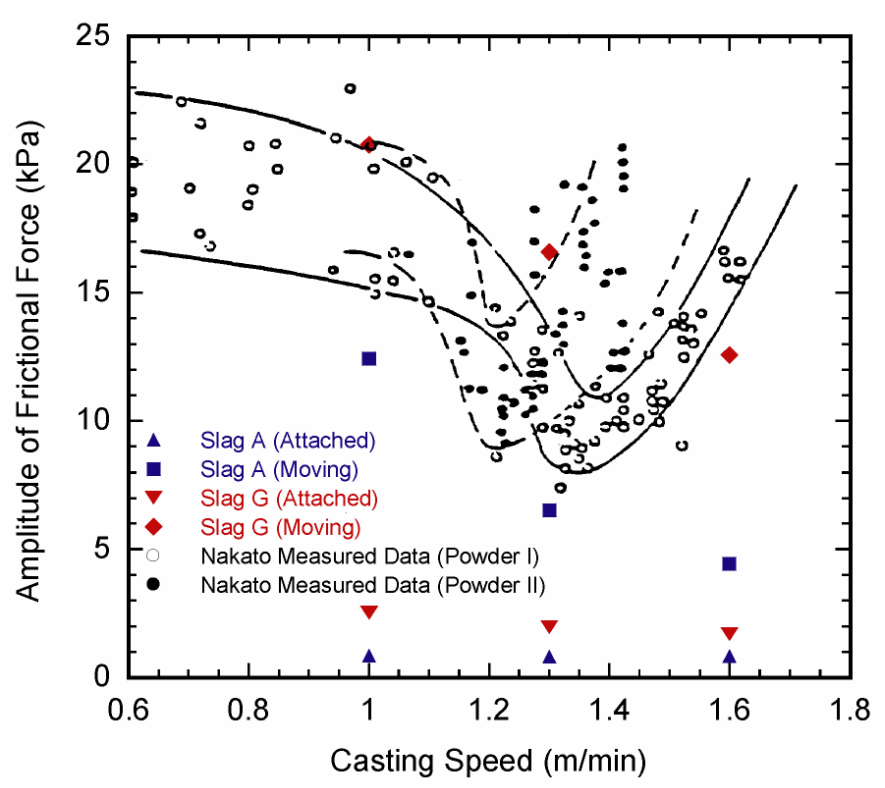

Fig. 24-Effect of casting speed on friction force: measurement and prediction